

NORTHWESTERN UNIVERSITY

Broadband Optical Cooling of Molecular Rotors

A DISSERTATION

SUBMITTED TO THE GRADUATE SCHOOL
IN PARTIAL FULFILLMENT OF THE REQUIREMENTS

for the degree

DOCTOR OF PHILOSOPHY

Field of Physics

By

Chien-Yu Lien

EVANSTON, ILLINOIS

August 2014

© Copyright by Chien-Yu Lien 2014

All Rights Reserved

ABSTRACT

Broadband Optical Cooling of Molecular Rotors

Chien-Yu Lien

Laser cooling of atoms is a widely utilized technique in scientific research, and has been developed over more than three decades. Recently, optically controlling and manipulating the external and internal degrees of freedom of molecules has aroused wide interest in the physics and chemistry communities. However, owing to the more complicated internal structure of molecules, laser cooling of molecules is still underdeveloped. Here we demonstrate cooling the rotation of trapped molecular ions from room temperature to 4 K. The molecule of interest, AlH^+ , is co-trapped and sympathetically cooled with Ba^+ to milliKelvin temperatures in its translational degree of freedom. The nearly diagonal Franck-Condon-Factors between the electronic X and A states of AlH^+ create semi-closed cycling transitions between the vibrational ground states of X and A states. A spectrally filtered femtosecond laser is used to optically pump the population to the two lowest rotational levels, with opposite parities, in as little as 100 μs by driving the A-X transition. In addition, a cooling scheme including vibrational relaxation brings the population to the $N = 0$ positive-parity level on the order of 100 ms. The population

distribution among the rotational levels is detected by resonance-enhanced multiphoton dissociation (REMPD) and time-of-flight mass-spectrometry (TOFMS). This technique opens new avenues to many further studies such as high-precision molecular quantum logic spectroscopy (mQLS) and fundamental constant measurements.

Table of Contents

ABSTRACT	3
Chapter 1. Introduction	7
Chapter 2. Experiment Overview	9
2.1. RF Linear Ion Trap and Laser Cooled Ba ⁺	9
2.2. Spectral Filtering of Broadband Laser for Rotational Cooling of Molecules	11
2.3. 1+1' REMPD and TOFMS	14
Chapter 3. RF Linear Ion Trap and Time-of-Flight Mass Spectrometry Apparatus	17
3.1. Ion Trap Design	17
3.2. Ion Trap Electronics and Toroid RF Resonator	18
3.3. Ion Optics (Einzel Lens) for Time-of-Flight Mass Spectrometry	20
Chapter 4. Rotational Cooling of Molecules Experiment	24
4.1. BROC Scheme	24
4.2. VA-BROC scheme	29
4.3. Rate-Equation Simulation	29
4.4. Experiment Procedure	30
4.5. Broadband Rotational Optical Cooling Result	33
Chapter 5. Conclusions and Future Directions	37

	6
5.1. Conclusions	37
5.2. Future Directions	38
References	41
Appendix A. Machine Drawing of Apparatus	47

CHAPTER 1

Introduction

Cooling is a procedure to reverse a dissipative process of a system in equilibrium with the environment at higher temperature, and can be achieved by many means. For instance, a system can be cooled with a cryogenic process using a liquid nitrogen or helium cryostat by direct contact with the system. One can also cool a system using a cold buffer gas, which involves cold gas particles taking phonons away from the system[**1, 2**]. Here in this dissertation I will introduce and elaborate upon an experiment designed to optically cool the rotational degree of freedom of the molecular ion AlH^+ [**3, 4**].

Preparing molecules in a specific quantum state is the key to many applications[**5**] such as molecular quantum logic spectroscopy (mQLS)[**6**], direct laser-cooling of molecules[**7, 8**], and ultracold chemistry[**9, 10, 11**]. Laser cooling of atoms[**12, 13, 14, 15**] has made possible many applications such as Bose-Einstein condensates and the all-optical atomic clock[**16**]. However, the additional rotational and vibrational internal structure of molecules as compared with atoms complicates laser cooling schemes. For typical diatomic molecules at room temperature (293 K), the population is distributed among many rotational and vibrational levels, each requiring an optical pumping laser at a unique wavelength in order to prepare the molecules in the rovibrational ground state.

Several groups have investigated coherent population transfer of loosely bound Feshbach states into the rovibrational ground state[**17, 18**]; however, since there is no dissipation (*e.g.*, spontaneous emission) in these schemes, state transfer does not cool the internal

degrees of freedom of molecules from a thermal distribution. There are currently two experimentally demonstrated approaches from the groups of M. Drewsen and S. Schiller to optically cool trapped polar molecular ions into the rotational ground state[**19, 20**]. Both drive specific vibrational transitions with narrowband IR lasers while relying on blackbody radiation to redistribute the population, achieving fractional rovibrational ground state populations about an order of magnitude higher than the room temperature equilibrium distribution in tens of seconds.

Optical cooling by a pulse-shaped femtosecond laser[**21**] has been employed to cool the vibrational population of neutral alkali dimers created from ultracold atoms by the group in Orsay, France[**22, 23**]. The same group discusses the possibility of using optical pulse-shaping for rotational cooling of Cs_2 [**22, 23**], but the required resolution, because of the small rotational constant, is far higher than the 1 cm^{-1} resolution achieved by them. In the later chapters, I would discuss the scheme of using a spectrally filtered (also called pulse shaped) broadband laser to optically cool the rotations of molecules with relatively large rotational constants comparing to Cs_2 . This scheme cools on an electronic transition with fairly diagonal Franck-Condon factors (FCFs)[**24**], such that electronic relaxation usually does not change the vibrational state. In particular, we demonstrate broadband rotational optical cooling (BROC) of AlH^+ molecular ions held in a room temperature radiofrequency (RF) linear ion trap as proposed in reference [**3**], and we furthermore demonstrate vibrational assisted BROC (VA-BROC) that cools rotations from 293 K thermal population distribution to a single rotational ground state in the same system.

CHAPTER 2

Experiment Overview

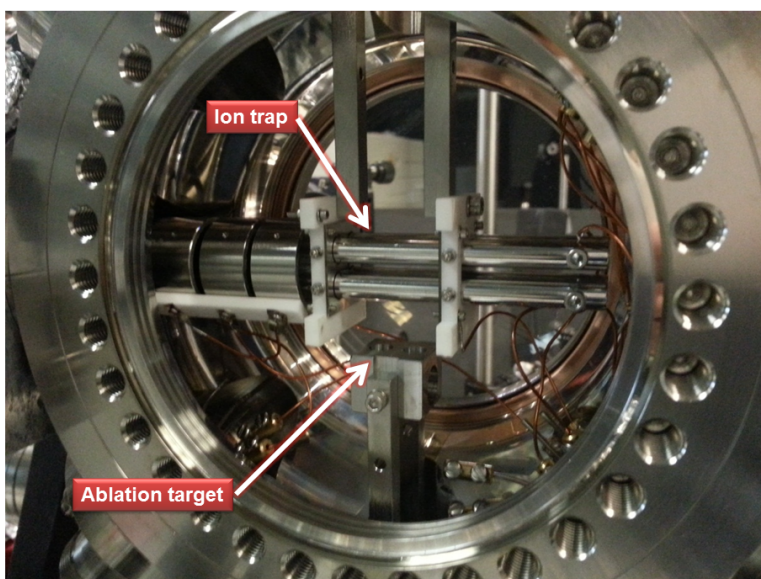
2.1. RF Linear Ion Trap and Laser Cooled Ba⁺

Figure 2.1. A RF linear ion trap designed to trap a wide range of ions with different masses by laser ablation loading.

To study and manipulate the internal degrees of freedom of molecular ions with the least possible interferences from the environment, an RF linear ion trap in an ultra-high vacuum ($\sim 5 \times 10^{-11}$ torr) chamber integrated with other apparatus was designed and utilized to load, confine and cool a variety of atomic and molecular ions with different masses.

Figure 2.1 shows the RF linear ion trap and targets for ablation loading in a vacuum chamber (Kimball Physics 6" Spherical Octagon). Further detail of the RF linear ion trap apparatus will be discussed in Chapter 3. Laser-ablation-loaded and laser-cooled Ba^+ ions[25, 26] are utilized to sympathetically cool the translational degree of freedom of the molecular ions[27]. Figure 2.2 shows a crystallized $^{138}\text{Ba}^+$ ion cloud and a Coulomb crystal formed with Ba^+ and AlH^+ .

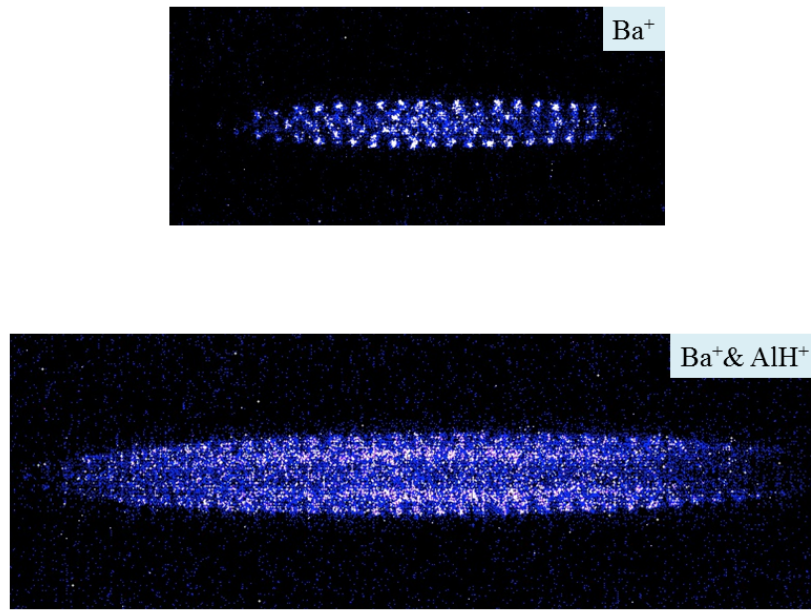


Figure 2.2. Upper panel: Laser-cooled and crystallized Ba^+ ions. The spacing between two Ba^+ ions is about $30 \mu\text{m}$ in the horizontal direction. Lower panel: Ba^+ and sympathetically cooled AlH^+ ions. AlH^+ ions experience stronger confinement from the radial RF field due to their lighter mass, and are shown as the dark core in this picture. The images are captured by an EMCCD camera (Photometrics Cascade:1K).

2.2. Spectral Filtering of Broadband Laser for Rotational Cooling of Molecules

Many approaches to cool the rotation of molecular ions are developed, and have different ultimate temperature and cooling time[**2, 19, 20**]. A scheme utilizing a spectrally filtered broadband laser (SFBL) to cool rotational degree of freedom of AlH^+ developed and realized in our lab[**3**] will be elaborated in Chapter 4. Here in this section I will discuss the setup and theoretical limit of the spectral filtering (also called pulse shaping[**21**]) of the broadband laser.

A home-built spectral-filtering (pulse-shaping) setup, consisting of diffraction gratings and cylindrical lenses in the 4-f Fourier-transform optical layout and a razor blade mask, is used to achieve spectral manipulation of the broadband laser[**3, 21, 28**].

On the Fourier plane, the spot size of any individual spectral color incident on the mask is given by[**21**]

$$(2.1) \quad w_0 = \frac{\cos \theta_{in}}{\cos \theta_d} \frac{\lambda f}{\pi w_{in}},$$

and the spatial dispersion (with units of distance/frequency) is given by[**21**]

$$(2.2) \quad \alpha = \frac{\lambda^2 f}{cd \cos \theta_d},$$

where λ is the wavelength, θ_{in} and θ_d are the incident and reflected angles from the grating, f is the focal length of the lens, d is the grating period, c is the speed of light, and w_{in} is the radius of the collimated beam incident on the grating.

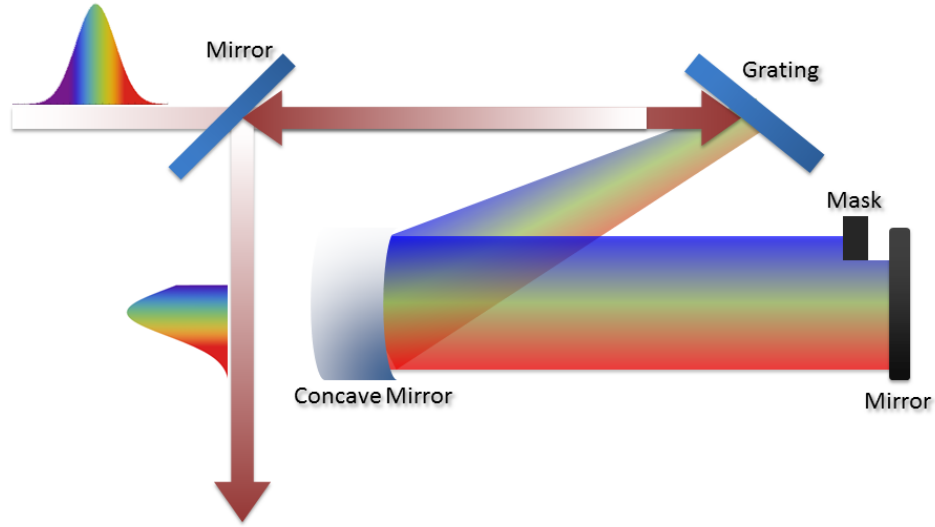


Figure 2.3. The schematics of so-called 4-f pulse-shaping setup to remove partial components of the broadband laser. The incoming broadband laser is diffracted by the grating, and collimated by the concave mirror (we actually use a mirror and a lens in the lab). The individual color components of the laser will be focused on the focal spot of the concave mirror, and that is also where the mask is to block the undesired color components. A mirror is placed behind the mask to retroreflect the broadband laser back with a slightly tuned vertical angle to allow another mirror to pick up the collimated laser beam.

The diffraction-limited full width at half maximum (FWHM) spectral resolution of spectral filtering is then given by[21]

$$(2.3) \quad \delta\nu_d = (\ln 2)^{1/2} \frac{w_0}{\alpha} = (\ln 2)^{1/2} \frac{\cos \theta_{in}}{\pi w_{in}} \frac{cd}{\lambda}.$$

Equation 2.3 shows that increasing w_{in} and decreasing d leads to better resolution, but this resolution is limited by the size of the optics. For a near-Littrow configuration ($\theta_{in} \sim \theta_d$) with $\lambda = 360$ nm, $d = 1/3600$ mm, and $w_{in} = 25$ mm, w_0 and $\delta\nu_d$ are $4.6 \mu\text{m}$ and 0.08 cm^{-1} , respectively.

The practical spectral resolution could be worse than $\delta\nu_d$ if the scale of mask features is limited to some size x . In that case, the mask-limited pulse-shaping resolution is given by

$$(2.4) \quad \delta\nu_m = (\ln 2)^{1/2} \frac{x}{\alpha} = (\ln 2)^{1/2} \frac{xcd}{\lambda^2 f} \cos \theta_d.$$

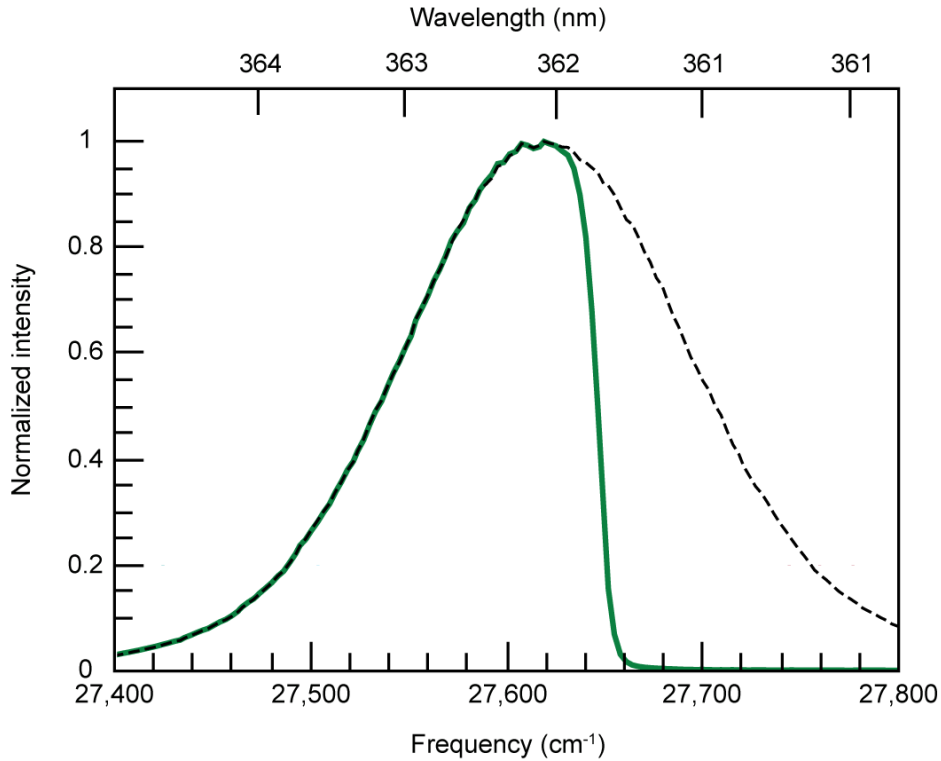


Figure 2.4. Spectral filtering a broadband laser. The black-dashed curve is the spectrum of the broadband femtosecond laser, and the green-solid curve is the spectrum of the broadband laser after spectral filtering.

This expression for δv_m is valid if $x > w_0$. Otherwise, different spectral colors on the Fourier plane would overlap, resulting in a smearing of the shaped profile. If a mask with 30 μm structure is used, $f = 1$ m, and the parameters given above, the expected spectral filtering resolution is 0.48 cm^{-1} , which is much better than the 10 cm^{-1} resolution required for AlH^+ BROC. For rotational cooling of SiO^+ molecules, 3 cm^{-1} resolution is required to pump only the cooling transitions (P-branch transitions in this case) while not exciting the heating transitions[8, 29]. Figure 2.4 demonstrates our current spectral filtering resolution to be better than 10 cm^{-1} , where the measurement is limited by the resolution of our spectrometer (Ocean Optics HR4000).

2.3. 1+1' REMPD and TOFMS

Evaluation of how well the molecular ions are prepared in the ground states is crucial; an accurate method is required to determine the population distribution among the rovibrational states. To this end, various approaches such as state-selective resonance-enhanced multi-photon dissociation (REMPD)[19, 20] and chemical reactions[30] have been used. We intend to use an already demonstrated method for state readout that counts the number of state-selectively photodissociated ions by sequentially dumping different species from the trap onto a detector[31].

AlH^+ ions in a specific rotational state of $X^2\Sigma^+(v = 0)$ will be optically excited to $A^2\Pi(v' = 0)$ with a tunable frequency-doubled pulsed dye laser (Sirah PrecisionScan) at a wavelength of 360 nm, and then excited to a dissociating state ($3^2\Sigma^+$) with a 266 nm pulse generated from the 4th-harmonic of an Nd:YAG laser (Continuum Minilite II). Because the first photon excites the population from one bound state to another, the excitation

process is state-selective. The two-photon-excited AlH^+ molecular ions dissociate into Al^+ ions and H atoms[31, 32, 33, 34].

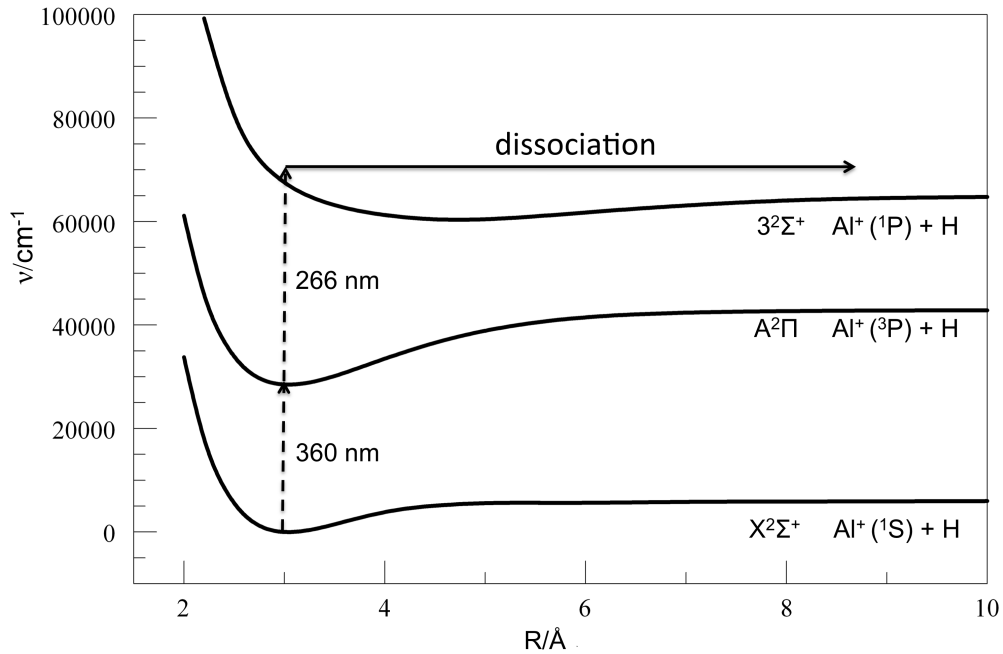


Figure 2.5. $1+1'$ Resonance enhanced multiphoton photodissociation. The population in the $X^2\Sigma^+(v=0)$ state is excited to a dissociating $3^2\Sigma^+$ level, through the intermediate state $A^2\Pi(v'=0)$.

This $1+1'$ REMPD rotational state readout scheme is destructive, and requires a technique to distinguish and quantify Al^+ and AlH^+ ions. In order to distinguish molecular and atomic ions after $1+1'$ REMPD, a few techniques are developed and studied in the lab, such as secular motion excitation[35, 36], Q-scan[37], and time-of-flight mass spectrometry (TOFMS)[38]. After many trials, we found that only TOFMS could provide the required mass resolution. Due to the only 1 Da mass difference between Al^+ (27 Da) and AlH^+ (28 Da), a carefully designed TOFMS apparatus that can extract ions out of

RF linear ion trap and yield 1 Da mass resolution was developed and implemented in our lab. Further details of this TOFMS apparatus can be found in Chapter 3 and reference [31].

CHAPTER 3

RF Linear Ion Trap and Time-of-Flight Mass Spectrometry

Apparatus

3.1. Ion Trap Design

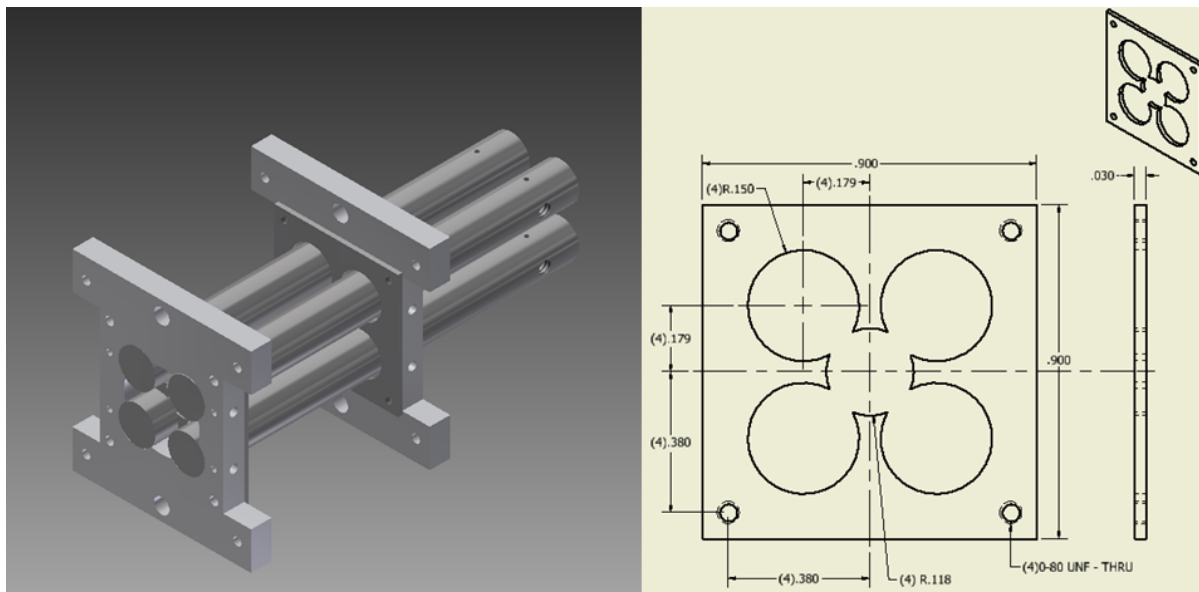


Figure 3.1. 3D drawing of ion trap assembly and machining drawing of endcap plate (dimension labels have units in inches).

To confine and hold atomic and molecular ions in a UHV chamber while allowing loading molecular ions, excess optical access, and TOFMS apparatus integration, an ion trap different from others in our lab[**25**, **26**] was designed, machined, and assembled to serve the versatile purposes. The left-hand side of figure 3.1 shows a 3D drawing of the ion trap assembly which consists of four stainless steel RF rods, two stainless steel endcap

plates, and two macor mounting plates. The endcap plate, with a hole at the center of it as shown on the right-hand side of figure 3.1, allows ions trapped in the ion trap to be extracted axially for TOFMS by changing the voltage applied on it. Complete machine drawings of the RF linear ion trap can be found in the Appendix.

3.2. Ion Trap Electronics and Toroid RF Resonator

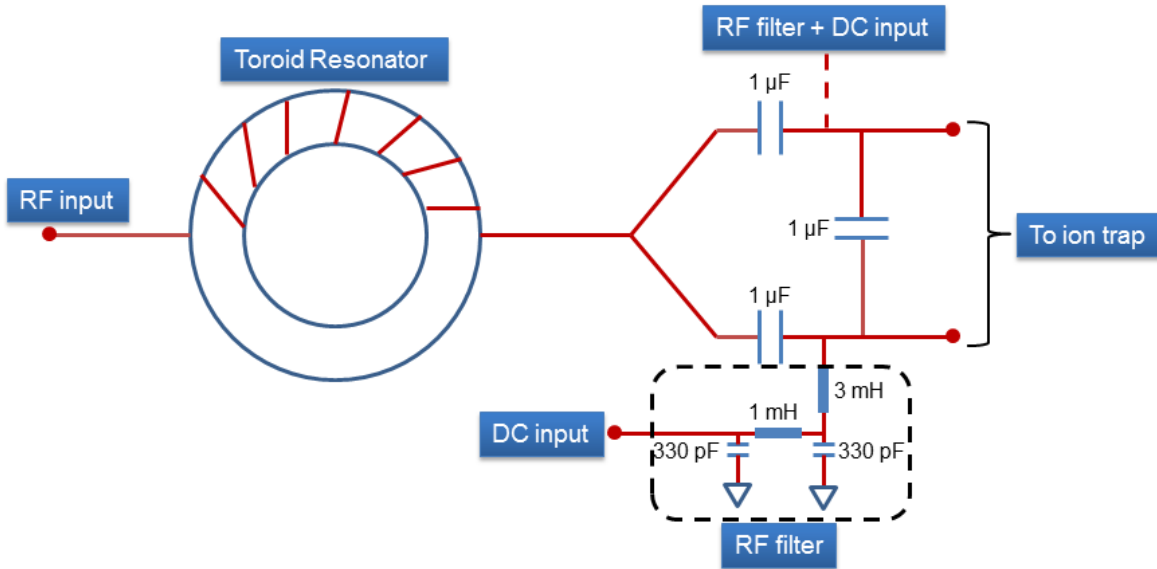


Figure 3.2. RF power supply electric circuit for the ion trap. The RF signal is generated by a function generator (Agilent 33220A), power amplified by a RF power amplifier (Mini-Circuits TIA-1000-1R8), and on resonance with the toroid resonator circuit shown in this figure. The two output pins of this circuit connect to one of the diagonal pairs of the RF rods of the ion trap, and could be added DC bias voltage independently. The typical RF peak-to-peak voltage (V_{pp}) applied to the RF rods is around 300-600 V_{pp} , and the typical DC bias used to compensate the patch potential in the ion trap is around 0.1 V.

To trap ions in a quadrupole RF ion trap, an RF source that provides amplitude of hundreds of voltage in a few MHz frequency is required. A home-built toroid resonator

with Q value around 20 was developed in the lab, and was also my very first project here in the Odom Lab. The idea is to design and create a toroid resonator that can transform low-voltage RF electrical waves into high-voltage RF electrical waves with a support of a 4 Watt RF power amplifier (Mini-Circuits TIA-1000-1R8).

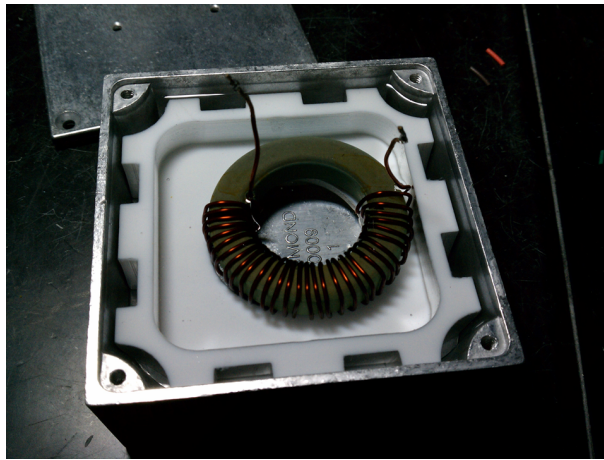


Figure 3.3. Toroid resonator. The toroid is submerged in mineral oil to stabilize its temperature and maintain a constant Q value.

Complete electronics for the ion trap system also involves several RF filters and DC input ports that allow adding compensation DC bias voltage to individual RF rods of the ion trap. Figure 3.2 shows the design schematics of the RF power supply electric circuit, and Figure 3.3 shows a picture of the toroid resonator resonating at around 3 MHz.

Besides RF voltage applied on the radial RF rods to form radial confinement of the ions, DC voltages are applied on the two endcap plates of the ion trap to provide axial confinement. DC voltages are powered by two high voltage power supplies (KEPCO BHK 2000-20MG), and the typical DC voltage applied on the endcap plates is around 800 V.

3.3. Ion Optics (Einzel Lens) for Time-of-Flight Mass Spectrometry

The ion cloud contains multiple species of atomic and molecular ions that are sympathetically cooled by the laser-cooled Ba^+ . A commonly used technique to distinguish the species is to excite the secular motion of the ions in the ion trap[27, 35, 36].

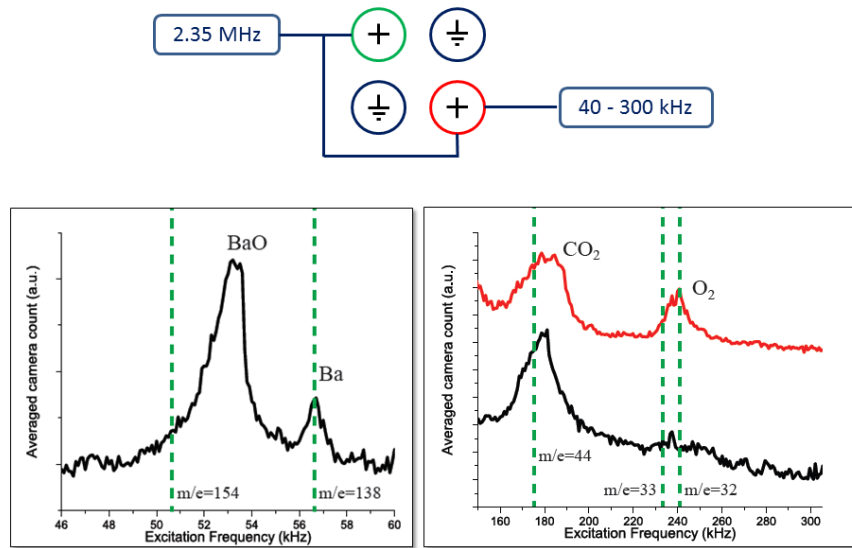


Figure 3.4. Secular excitation of different species in the RF linear ion trap. The top panel shows how the excitation voltage (40 - 300 kHz) is applied on top of the RF frequency (2.35 MHz) used to trap the ions. The lower panel shows two spectra of secular excitation. The resonance peaks of ions other than Ba^+ are shifted due to the interference of Ba^+ .

Figure 3.4 shows two spectra of exciting the secular motion of non-laser-cooled species, BaO^+ , CO_2^+ , and O_2^+ , radially. A small voltage (~ 0.1 mV) is applied to one of the RF rods to provide a tiny fluctuation of electric field to excite the radial secular motion of ions. Because the cooling laser of Ba^+ is far-red detuned, while the ion cloud is hotter because the motion of trapped ion species is on resonance with secular excitation, the

more fluorescence photons are emitted from the Ba^+ ions and collected by the EMCCD camera.

Unfortunately, the secular excitation technique cannot provide enough mass resolution to distinguish Al^+ and AlH^+ ; therefore, the signal of the rotational cooling of AlH^+ are analyzed by a time-of-flight mass spectrometry apparatus integrated with the RF linear ion trap, introduced in the earlier sections. Ions in the ion trap are extracted by rapidly lowering the voltage (in 10 ns) applied to one of the endcap plates of the ion trap from around 900 V to -150 V.

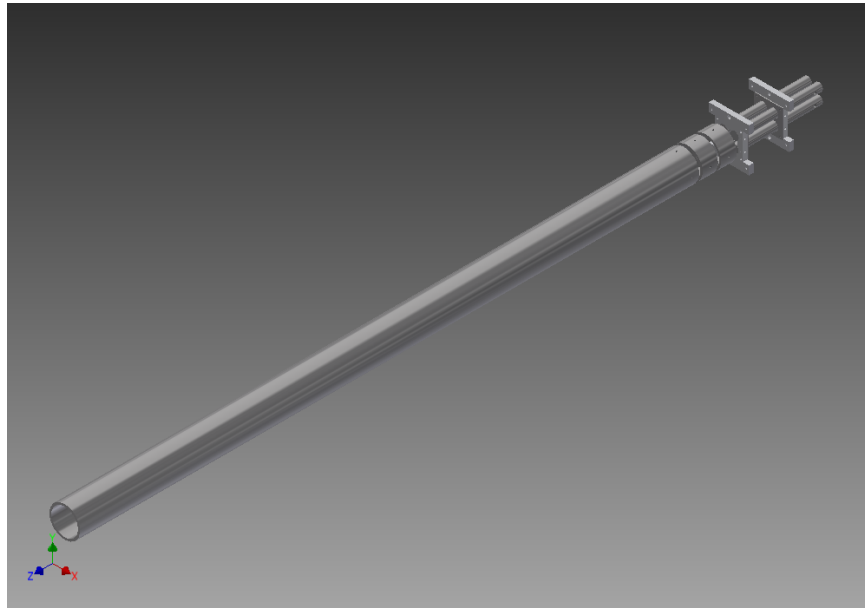


Figure 3.5. 3D drawing of the RF linear ion trap assembly integrated with the TOFMS apparatus. The TOFMS apparatus includes a set of einzel lens to focus ions transversely, a flight tube to provide a field-free region, and an micro-channel plate (Hamamatsu F4655, not shown in this figure) to convert ions into electrons.

Even the ion cloud is laser cooled to sub-Kelvin temperature, the ions diverge drastically while they are extracted from the ion trap as a result of the Coulomb repulsion

between ions and the lack of radial confinement. Therefore, a set of ion optics (einzellens[39]) is utilized to focus ions transversely right after they leave the ion trap. Figure 3.6 shows ion trajectories while ions are released with different initial condition, *i.e.*, different positions in the ion trap.

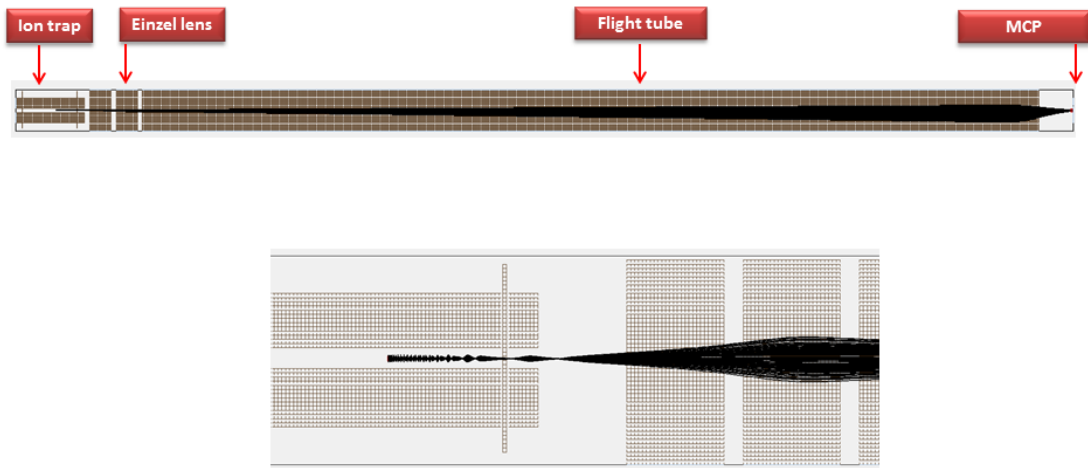


Figure 3.6. TOFMS ion trajectories simulated by SIMION. The top panel shows the ion trajectories of the ions when they are ejected from the ion trap and fly toward the micro-channel plate (MCP). The lower panel shows a zoom-in view around the exit of the ion trap. The einzel lens focus the ions transversely since ion trajectories diverge quickly right after they leave the ion trap. The ion trajectories shown in the figure contain 500 ions released in 500 random positions in the range of $\pm 500 \mu\text{m}$ in axial direction and $\pm 200 \mu\text{m}$ in radial direction from the trap center.

Besides focusing the ion cloud laterally, we also developed a technique to focus the ion cloud in the axial direction. We call it “time focus” because this technique reduced the distribution of the ion time-of-flight, and enhanced the time resolution of the TOFMS.

Figure 3.7 shows a schematic of the idea of this time focus technique. Due to the non-negligible size of the ion cloud in the axial direction of the ion trap, the TOFMS

signal of a single mass ion cloud could spread out over a few microseconds. By tuning the voltages applied on the two endcap plates of the ion trap, optimized voltages could be found to make the ions, of the ion cloud, closer to the ion detector arrives ion detector simultaneously with the ones further away from the ion detector. The optimized voltages for TOFMS for ions with mass around 27 Da are 875 V and -140 V for the endcap plates further and closer to the ion detector, respectively.

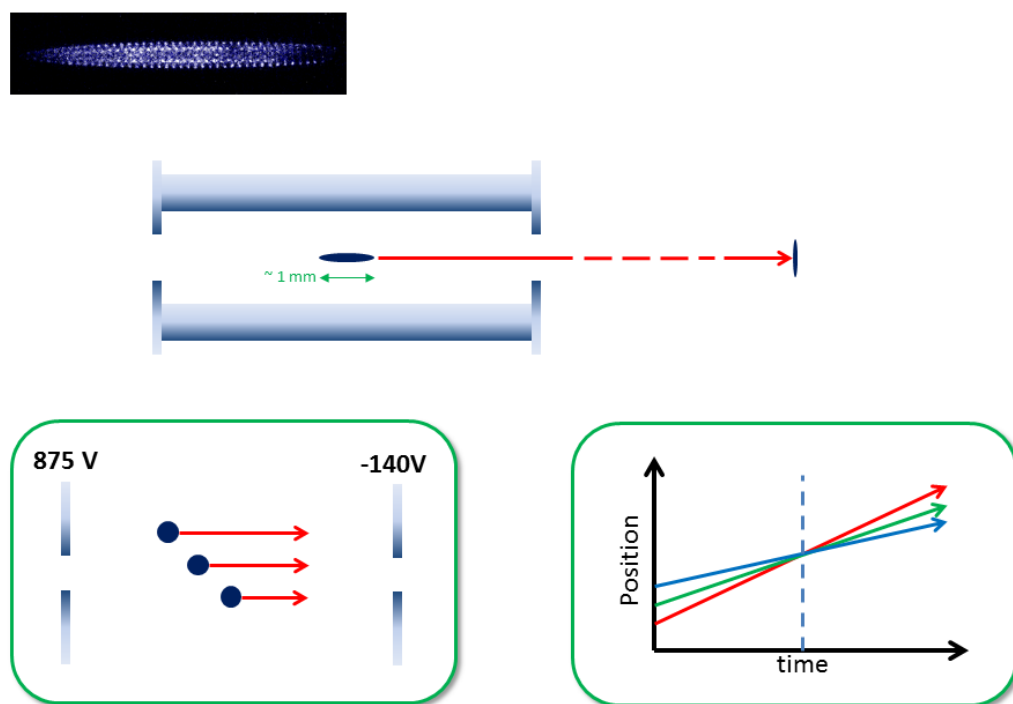


Figure 3.7. Time focus of the TOFMS.

CHAPTER 4

Rotational Cooling of Molecules Experiment**4.1. BROCC Scheme**

To manipulate internal degrees of freedom of molecules, one would have to consider not only the electronic transitions, but also vibrational and rotational transition (Figure 4.1 **a.**). While reaching equilibrium with the environment (293 K), population in diatomic hydride molecules such as AlH^+ would be mostly in the vibrational ground states due to the $>1000 \text{ cm}^{-1}$ energy gap between $v = 0$ and $v = 1$ in the electronic ground state $\text{X}^2\Sigma^+$; however, most of the population would distribute among ten or more of rotational states.

The previously-demonstrated optical-rotational cooling schemes[**19, 20**] used infrared CW lasers to drive a small number of vibrational transitions, requiring on the order of tens of seconds for polar hydride molecules in a 300 K environment to reach equilibrium. For hydrides, these schemes are limited to seconds timescales by blackbody-radiation-induced rotational transition rates, and are in principle limited by the vibrational relaxation times of tens of milliseconds. Electronic transitions are generally much faster than rotational and vibrational transitions; for example, the decay $\text{A}^2\Pi(v' = 0) \rightarrow \text{X}^2\Sigma^+(v = 0)$ for AlH^+ occurs with a time constant of 10^{-7} s, as compared with the 10^{-1} s for $\text{X}^2\Sigma^+(v = 1) \rightarrow \text{X}^2\Sigma^+(v = 0)$. Unlike for vibrational excitation approaches, extension of our scheme to molecules with larger reduced mass (non-hydrides, *e.g.*, SiO^+ [**8**]) is also possible without

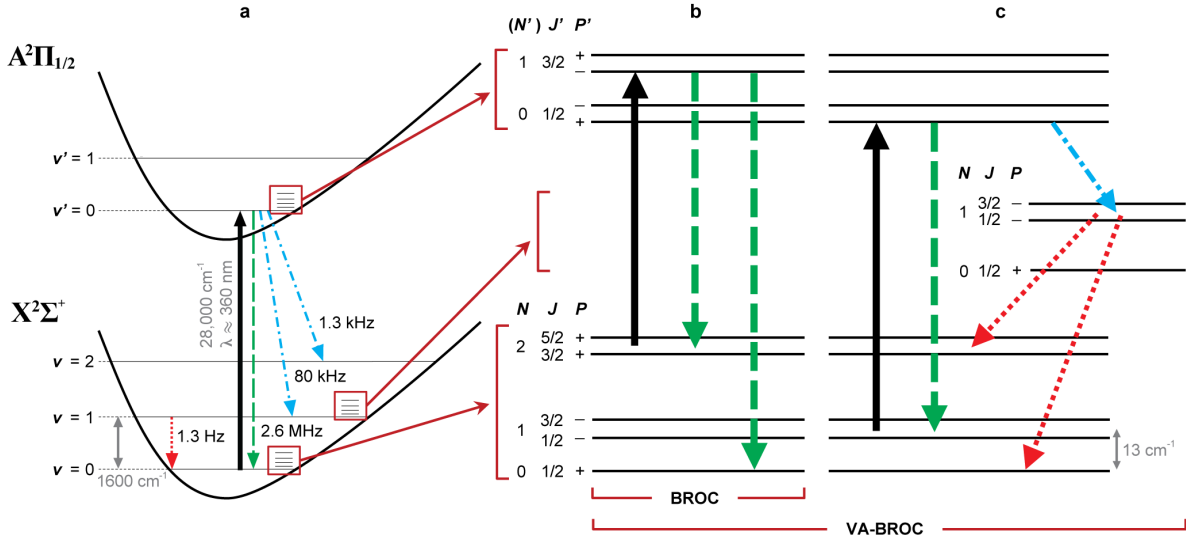


Figure 4.1. This figure shows the transitions between two electronic states and vibrational states within the electronic ground state. The stimulated absorptions are shown in solid arrows, and spontaneous emissions are shown in dashed arrows. **a.** Electronic transition between $A^2\Pi(v' = 0)$ and $X^2\Sigma^+(v = 0)$ states allows many cycling transitions before the population falling to $v > 0$ vibrational states. **b.** BROC. In this two-photon process cooling scheme, the SFBL drives multiple P-branch transitions to pump the population into lower rotational levels. Here the figure shows one of the P-branch transitions used for cooling and the possible decay channels from the upper state. This cooling scheme will pump the population to the two lowest rotational levels with opposite parity. **b & c.** VA-BROC. By tuning the spectral filter of SFBL, extra components of the SFBL would be used to drive the population from $|v = 0, N = 1\rangle$ to $|v = 1, N = 1\rangle$, and the vibrational relaxation will bring the population to $|v = 0, N = 2\rangle$ and $|v = 0, N = 0\rangle$. This three-photon process flips the negative parity of $|v = 0, N = 1\rangle$

incurring longer cooling times. The nearly diagonal FCFs between the electronic X and A states of AlH^+ create semi-closed cycling transitions between the vibrational ground states of X and A states.

The broadband rotational optical cooling scheme uses a SFBL to pump the population of diatomic molecular ions (*e.g.*, AlH^+) trapped in a RF linear ion trap, to their

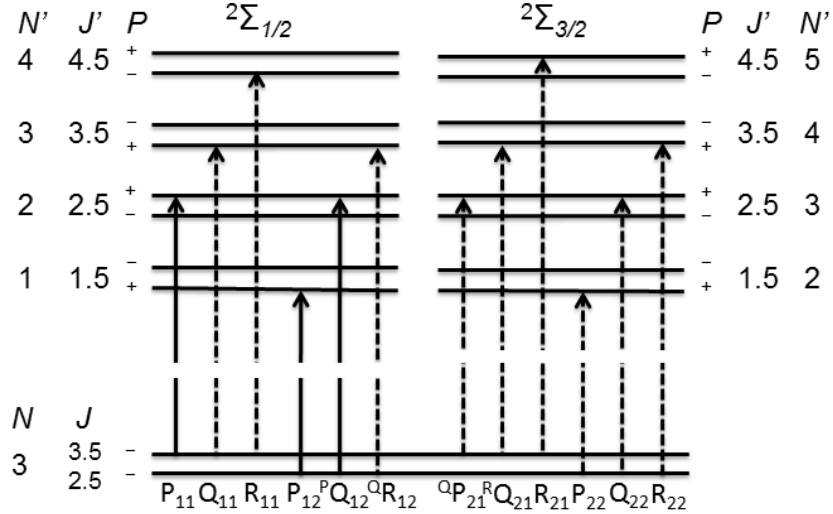


Figure 4.2. All transitions which could be driven from an example state, $N = 3$. Pulse shaping removes wavelengths corresponding to dashed lines in the figure.

rovibrational ground states. Because a SFBL can pump many of the internal cooling transitions simultaneously, no blackbody radiation is required for redistributing the population among rotational states. Cooling is accomplished by a sequence of photon absorption events, each followed by a spontaneous emission; throughout the process, the SFBL spectrum is not adjusted. Since the highly diagonal FCFs of AlH^+ [40] (see Figure 4.1 a.) limit the population leakage, during electronic decay, to higher vibrational states, only one SFBL is required. For other molecules with less diagonal FCFs, a second SFBL tuned to repump the excited vibrational populations could be added.

The $\text{AlH}^+ \text{A}^2\Pi(v' = 0) \rightarrow \text{X}^2\Sigma^+(v = 0)$ spectra in Figure 4.3 are calculated using the molecular Hamiltonian provided in Almy and Watson's work[33], and the molecular constants calculated by Guest *et.al.* and Szajna *et.al.*[32, 41]. The angular momentum

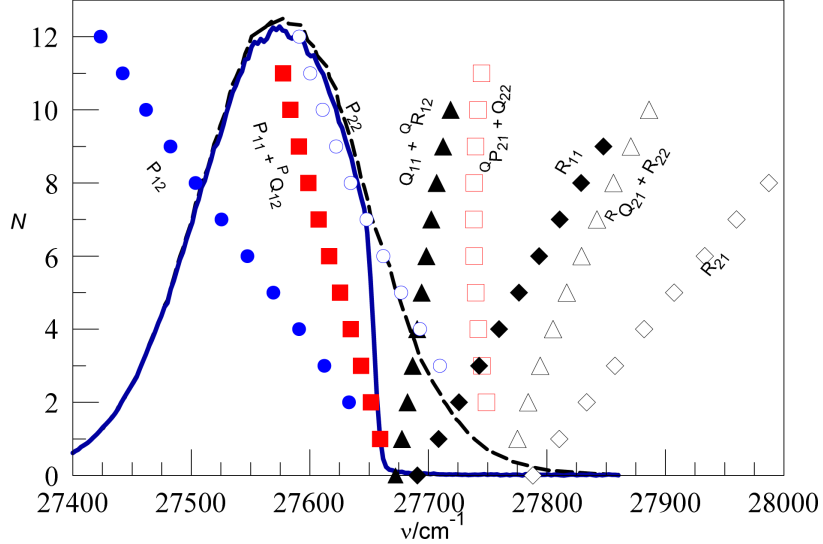


Figure 4.3. PROC for AlH^+ . The pulse-shaped frequency-doubled femtosecond laser (solid-blue line, data) with a cutoff at $27,655 \text{ cm}^{-1}$ can be used for branch-selective optical pumping, cooling the rotational degree of freedom. The closed and open symbols represents the F_1 and F_2 transitions, respectively. The dashed line shows the femtosecond laser spectrum without pulse-shaping. The population among $N = 2 - 12$ rotational levels will be pumped to the dark states, $N = 0, 1$ (see text for details).

selection rules for the transition between $A^2\Pi$ and $X^2\Sigma^+$ are $\Delta J = 0, \pm 1$, where $\mathbf{J} = \mathbf{N} + \mathbf{S} + \mathbf{L}$ is the total angular momentum including molecular rotation \mathbf{N} , electron spin \mathbf{S} , and orbit \mathbf{L} . The SFBL drives only selected P- and Q-branch transitions (see Figure 4.2) as shown in Figure 4.3, which will result in rotational cooling and not heating. This arrangement creates dark states: the two rotational ground states, $X^2\Sigma^+|v = 0, N = 0\rangle$ and $X^2\Sigma^+|v = 0, N = 1\rangle$. The population of the two dark states cannot be transferred from one to the other through a two-photon process because of parity.

Our broadband laser (SpectraPhysics MaiTai) has an 80 MHz repetition rate, so each pulse has a comb-like frequency spectrum with frequency interval equal to the repetition

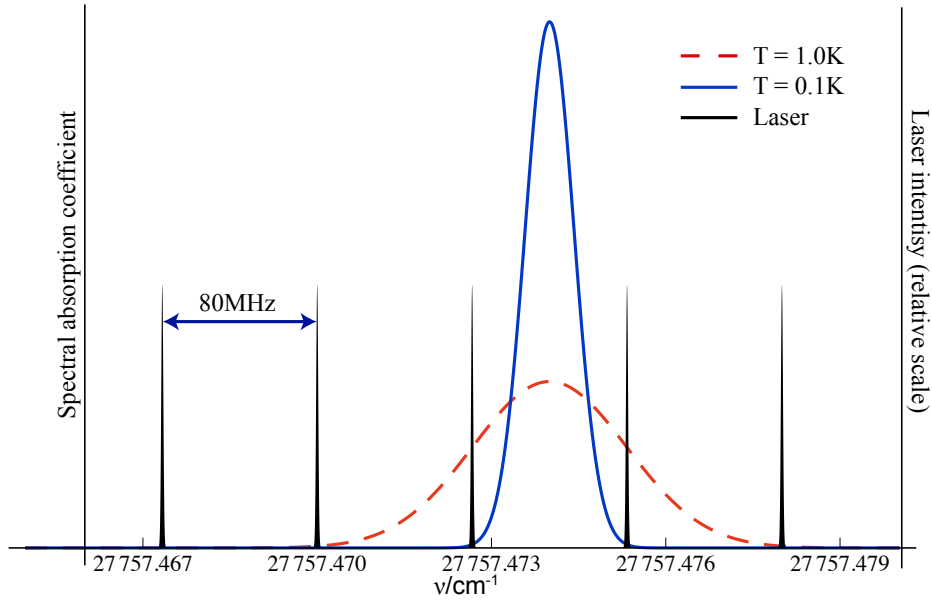


Figure 4.4. Doppler broadening helps the overlap between the SFBL and the transition linewidth.

rate. The linewidth of $\text{AlH}^+ \text{X}^2\Sigma^+(v=0) \rightarrow \text{A}^2\Pi(v'=0)$ transitions is of order $1/60 \text{ ns}^{-1}$ ($2\pi \times 3 \text{ MHz}$), which is smaller than the comb interval; therefore, it would be possible for the SFBL to miss some of the transitions we desire to pump. The simplest solution to this issue is to increase the translational temperature of the AlH^+/Ba^+ ion cloud (see Figure 4.4), since a modestly Doppler-broadened linewidth ensures that the SFBL can drive all the desired cooling transitions. One broadening approach is to directly excite the secular motion of the AlH^+ with an oscillating electric field. After internal cooling is finished, the secular drive is turned off, and the translationally hot molecular ions are again sympathetically cooled by the laser-cooled Ba^+ . Another approach to temporarily increase the linewidth of the molecular ions is to push the entire ion cloud away from the geometric center of the Paul trap by applying a DC field. This displacement introduces excess micromotion[42], where the ions undergo swift oscillations at the RF frequency

with amplitude proportional to the applied DC field. To reach the desired linewidth broadening (80 MHz) in the geometry of our trap ($r_0 = 3$ mm, $\Omega \sim 2\pi \times 3$ MHz), the ions have to be pushed only $2 \mu\text{m}$ away from the geometric trap center.

4.2. VA-BROC scheme

In addition to the BROC scheme that cools rotations of molecules to the two lowest levels, another cooling process, shown in Figure 4.1 **c.**, utilizing the vibrational decay, from $v = 1$ to $v = 0$, to flip the parity via a 3 photon process was developed and demonstrated in our lab. This vibrational assisted broadband rotational cooling (VA-BROC) scheme cools the rotations of AlH^+ to the single lowest rotational level, $N = 0$, by introducing extra components of the SFBL by tuning the spectral filter setup to pump the population from $|v = 0, N = 1\rangle$ to $|v = 1, N = 1\rangle$ in 100 microseconds, and the vibrational relaxation brings the population from $|v = 1, N = 1\rangle$ to $|v = 0, N = 0\rangle$ in the order of 100 milliseconds.

4.3. Rate-Equation Simulation

We modeled BROC and VA-BROC for AlH^+ using a rate-equation simulation. Results of simulating BROC are shown in Figure 4.5. The simulation simulates with 1/10 of saturation intensity driving the cooling transition which is limited by the SFBL laser power, and hence cools the rotations via BROC process slower than the ideal case shown in reference [3]. The simulation shows that BROC achieves 63% ($1 - e^{-1}$) of population saturation in $8 \mu\text{s}$, with an accumulated population in the lowest two rotational states, $|v = 0, N = 0\rangle$ and $|v = 0, N = 1\rangle$, of 86% in $25 \mu\text{s}$. The different equilibrium populations

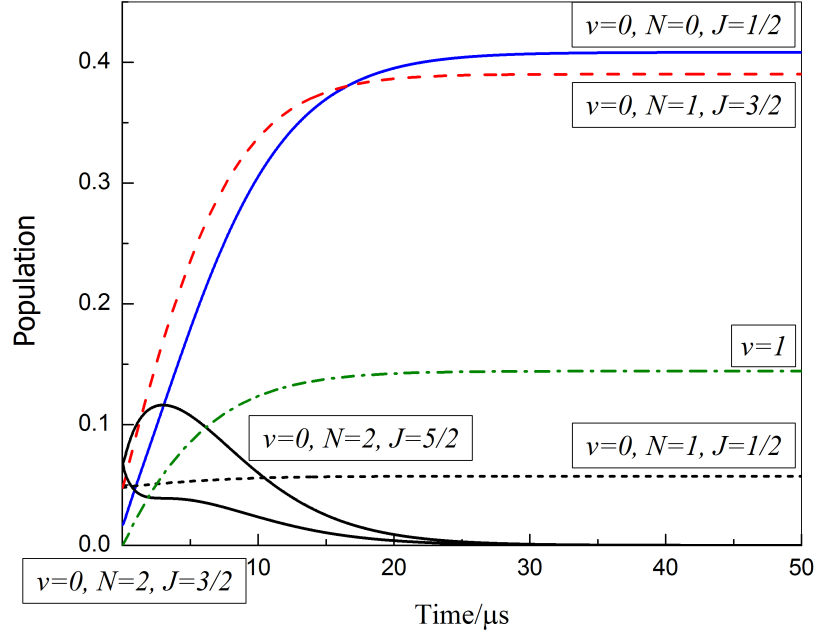


Figure 4.5. Simulation results of BROCC for the time evolution of the lowest five spin-rotational levels in $v = 0$ and the total population in $v = 1$.

of the dark states in Figure 4.5 reflect the number of spontaneous decay channels feeding into each state.

4.4. Experiment Procedure

The 532 nm pulse laser (Continuum Minilite II) ablates the Barium target and created a plume of Barium neutrals and ions into the ion trap while the electronics of the ion trap is on. The Ba^+ ions are laser cooled and trapped in the ion trap, and subsequently Coulomb crystallized into an ion cloud near the absolute zero temperature in a few seconds as shown at the bottom right corner of Figure 4.6. After loading Ba^+ ions, the 532 nm pulse laser ablates Aluminum target to load Al^+ ions with higher power comparing to the

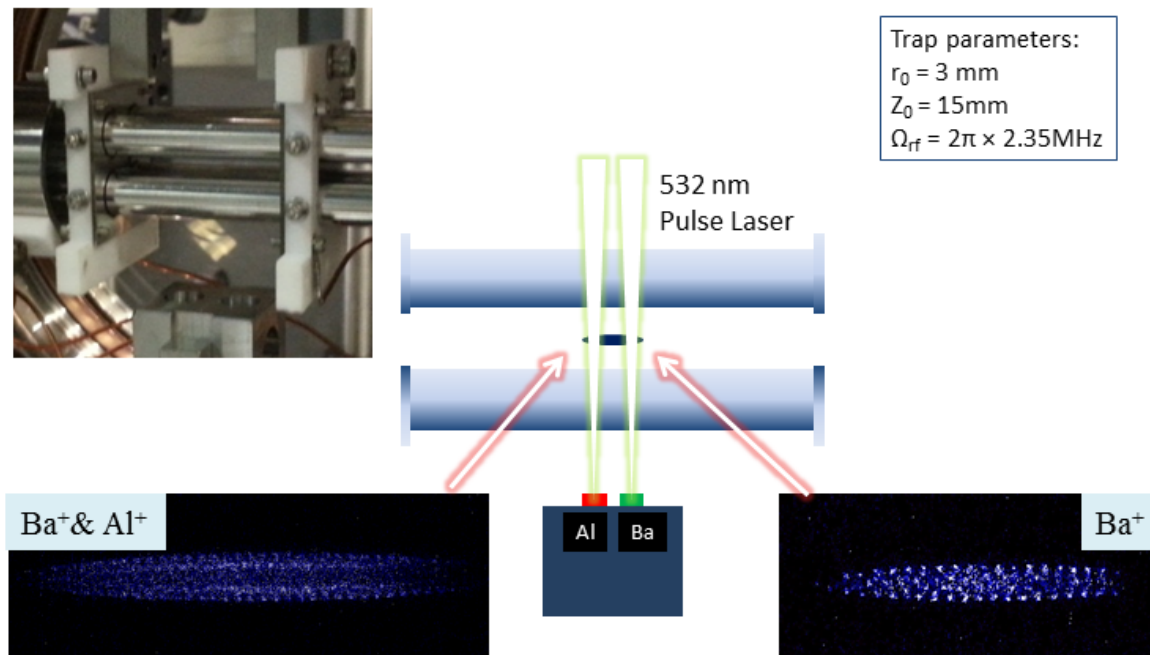


Figure 4.6. RF linear ion trap and laser ablation loading. Two pulse laser beams ablate Ba and Al targets with different power.

one loading Ba^+ ions. The Al^+ ions are sympathetically cooled with Ba^+ ions, and form the dark core of a Coulomb crystal, as shown at the bottom left corner of Figure 4.6, since Al^+ ions have smaller mass and experience tighter radial confinement comparing to Ba^+ ions. There are typically 50 Al^+ ions in each experiment run to maintain good TOFMS resolution.

After a few minutes the ablation loaded Al ions react with background gas, and turn into AlH^+ ions. The SFBL (SpectraPhysics Mai Tai) and 1+1' REMPDL lasers (Sirah

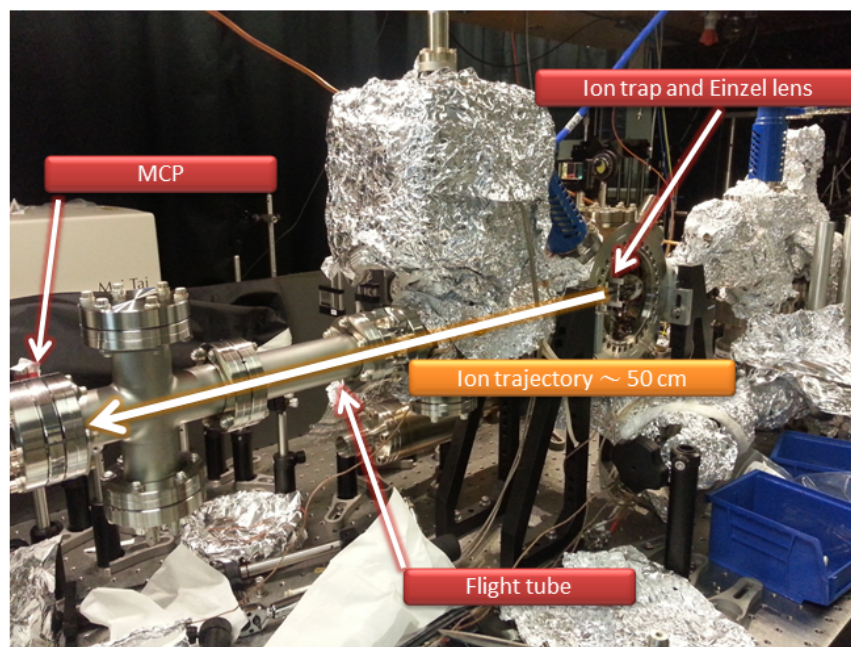


Figure 4.7. Picture of TOFMS apparatus. Ions are extracted from the ion trap, focused laterally by the ion optics, fly through the field-free region (flight tube), and finally arrive and are detected by the MCP.

PrecisionScan & Continuum Minilite II) would be shined into the ion trap in sequence to cool the rotations and state-selectively photodissociate AlH^+ as described in the earlier sections and reference [31]. The REMPD lasers photodissociate a portion of AlH^+ ions that the population are in the selected rotational quantum states into Al^+ ions and H atoms, and the AlH^+ would remain trapped and sympathetically cooled with Ba^+ and other AlH^+ in the ion trap. A few seconds later the Coulomb crystal would be extracted by changing the voltage applied on one of the endcap plates (from 850 V to -140 V in 10 ns). The ions would be focused laterally by the Einzel lens (see Chapter 3 for details), enter a field free region called flight tube, and finally hit the MCP to yield current signal

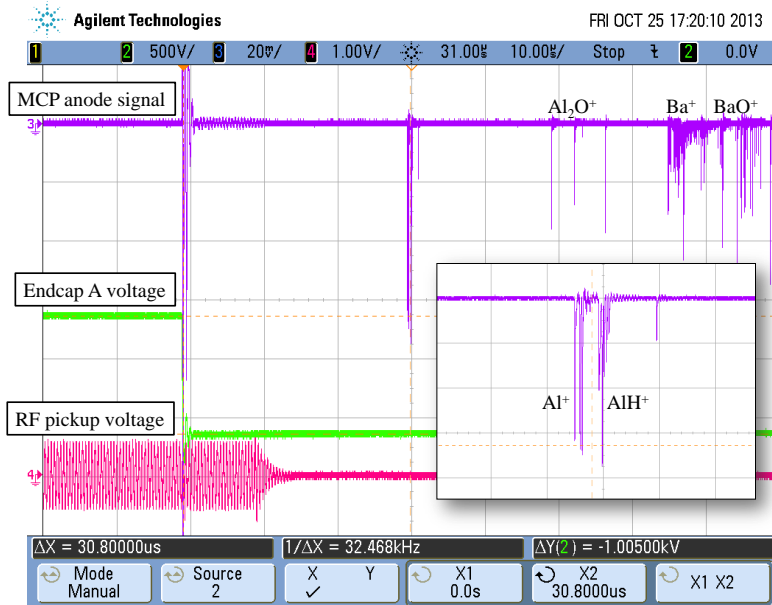


Figure 4.8. Sample TOFMS sepctrum. An ion cloud containing multiple species of ions is extracted from the ion trap by ramping down voltage applied to an endcap plate (green curve). The purple curve represents current signal detected by the anode of MCP assembly. The inset shows the zoom-in view of the peaks at the center of the figure, and the signals between Al^+ and AlH^+ are separated around 500 ns. The red curve is the pickup signal of RF voltage applied to the ion trap, and we found turning the RF voltage off help improve Signal-to-noise ratio of the TOFMS measurement.

detected by the anode of MCP assembly. Figure 4.8 shows a sample TOFMS spectrum. The analog-mode MCP signal is measured by an oscilloscope with a sample rate of 2 GSa/s (Agilent DSO7014A). Further detail of the experiment including quantifying the number of ions detected by the MCP can be found in reference [31].

4.5. Broadband Rotational Optical Cooling Result

Figure 4.9 a. shows the evolution of the population during different cooling process, BROCC and VA-BROCC. As elaborated in the previous sections, BROCC cools molecules

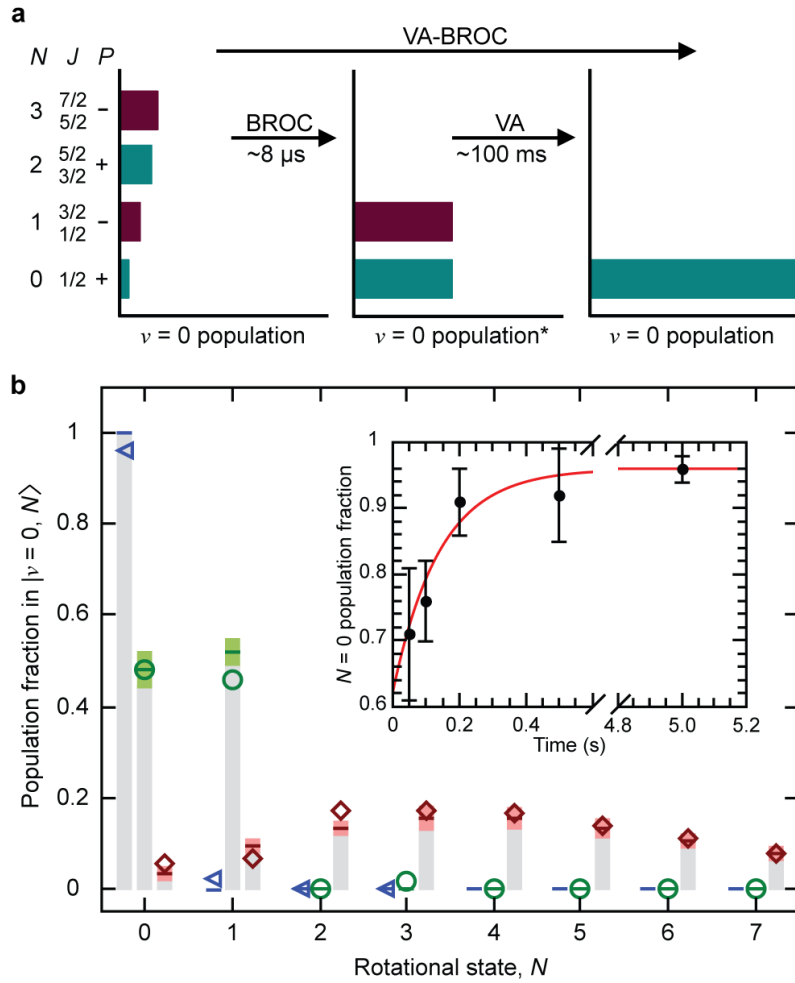


Figure 4.9. BROC and VA-BROC result. **a.** Population distribution before cooling (at 293 K), after BROC, and after VA-BROC. *14% of population is in $\nu > 0$ states, and takes ~ 100 ms to spontaneously decay back to $\nu = 0$. **b.** Population distribution among rotational states, N . The red diamonds, green circles, and blue triangles represents population in specific N states at room temperature, after BROC, and after VA-BROC, respectively. The horizontal lines are the theoretical prediction of the population distributions with the colored bands denoting the 60% confidence region. The inset shows population in the $N = 0$ state after various VA-BROC duration, and the red curve is a fit to the data points using equation 4.1.

to the two lowest rotational state, $N = 0, 1$, and VA-BROC in additionally pumps the population in the negative parity state, $N = 1$, to the positive parity state, $N = 0$. in the

order of vibrational lifetime, τ . Figure 4.9 **b.** shows the experimental result of running 5 s BROCC and VA-BROCC procedure. BROCC procedure cools rotations from the room temperature (293 K) thermal population distribution to the two lowest rotational states, and results in 48(4)% and 46(3)% population in $|X^2\Sigma^+, v = 0, N = 0\rangle$ and $|X^2\Sigma^+, v = 0, N = 1\rangle$, respectively. Although the plot shows non-zero population in $N = 3$ after BROCC, which could be caused by inefficiency or dissociation loss; however, the signal is most likely from detector noise such as MCP dark current. After VA-BROCC, the population measured in $|X^2\Sigma^+, v = 0, N = 0\rangle$ is $95_{-2.1}^{+1.3}\%$; probing $|X^2\Sigma^+, v = 0, N = 1\rangle$, we measure a population of $2.0_{-1.4}^{+3.3}\%$, and we observe no population in $N = 2$ or $N = 3$.

Because the limited opening period of the mechanical shutters controlling the SFBL and REMPD lasers, population dynamics measurements are limited to 10 ms, and cannot retrieve the 8 μ s BROCC cooling time predicted in the rate equation simulation introduced in the earlier section. The data shown in the main plot of Figure 4.9 **b.** are measured with 5 s SFBL on time. Nevertheless, the 10 ms shutter period allows us to measure the population evolution under various SFBL on-time in the VA-BROCC procedure, as shown in the inset of Figure 4.9 **b.**, to test the limit of this procedure and extract the vibrational relaxation time from $v = 1$ to $v = 0$ in $X^2\Sigma^+$ state of AlH^+ .

In VA-BROCC, the SFBL pumps the population out of $|v = 0, N = 1\rangle$ to $|v = 1, N = 1\rangle$ in hundreds of microseconds, and the vibrational relaxation brings population to $|v = 0, N = 2\rangle$ and $|v = 0, N = 0\rangle$ in the order of τ , about 100 milliseconds. Population in the $|v = 0, N = 0\rangle$ stays there until BBR drives it out to other states; however, population in $|v = 0, N = 2\rangle$ would be pumped to $|v = 0, N = 0\rangle$ through the BROCC process in a few

microseconds. Therefore, the dominate timescale of VA-BROC process is the vibrational relaxation time, τ .

Similarly to the approach used in [43], τ can be extracted from time-dependent population. An equation is derived to describe and fit the measured population in $v = 0, N = 0$ state under various SFBL on time.

$$(4.1) \quad P(t) = P_{total} - P_{N=1}(0)B_2e^{-t/\tau}$$

$P(t)$ represents the population in the $N = 0$ level after the molecule is pumped by the SFBL for various duration t . P_{total} is the parity pumping efficiency for 5 s SFBL on time. $P_{N=1}(0)$ is the initial population in $N = 1$ level. B_2 is the branching fraction of population in $|v = 1, N = 1\rangle$ decay to $|v = 0, N = 2\rangle$ calculated with Hönl-London factors. τ is the spontaneous decay lifetime from $v = 1$ to $v = 0$.

The fit shown in the inset of Figure 4.9 **b.** using this equation yields a τ of 140(20) ms, which is in a good agreement with the theory value of 127 ms[40].

CHAPTER 5

Conclusions and Future Directions**5.1. Conclusions**

Optical cooling of molecular ions to a single rotational state is demonstrated. The internal temperature of the molecular ions can be cooled with a spectrally filtered broadband laser to 4.7 K (95% population in the rotational ground state) as fast as 140 ms. The population distribution among rotational levels is analyzed with a combination of two techniques, REMPD and TOFMS, as described in the earlier chapters. Currently another project in our lab is investigating fluorescence imaging of molecular ions as an alternative and non-destructive state readout method.

Lower rotational temperature is expected with improved spectral filtering. A rate equation simulation predicts that for operating VA-BROC below saturation on all transitions, if 1% of the intensity pumping $P(N = 1)$ leaks through the filter to pump $Q(N = 0)$ would result in 6% population in $N = 1$, similar to the measured quantities shown in Figure 4.9. The separation between the $P(N = 1)$ and $Q(N = 0)$ transitions is 13 cm^{-1} (390 GHz), and the spectral filtering resolution of the current setup is 2 cm^{-1} (60 GHz), measured from peak transmitted intensity to $1/e^2 = 14\%$. A few percent of the intensity driving $P(N = 1)$ might not be blocked completely and driving $Q(N = 0)$, and result in imperfection of VA-BROC.

The rotational cooling technique is also applicable to other candidate species have diagonal FCFs[8, 40]. Additionally, with broadband vibrational cooling technique[22, 23], the BROCC and VA-BROCC can be applied to molecular species with non diagonal FCFs.

5.2. Future Directions

After achieving cooling the rotations of molecules, one can apply this technique to a variety of studies[5, 44]. Here I would like to elaborate on one of the many interesting applications, molecular quantum logic spectroscopy (mQLS). Since we have the technique to prepare a molecular ion in a specific quantum state, the molecular precision spectroscopy utilizing a scheme proposed by P. O. Schmidt's group[45] to measure the frequency of a transition of a molecule to much greater accuracy (1/300 of the observed linewidth of AlH^+ A-X transition is tens of kHz) comparing to current spectroscopy data ($0.006 \text{ cm}^{-1} \sim 200 \text{ MHz}$)[41].

Figure 5.1 shows the schematics for a mQLS experiment. A laser-cooled atomic ion is co-trapped with a molecular ion of interest[46]. After cooling this two-ion system to Doppler cooling limit[12], apply resolved sideband cooling[15, 47, 48] on the atomic ion to cool the center-of-mass (COM) mode of the system to motional ground state. Short pulses of spectroscopy light would be shined, with the repetition rate synchronized to the normal mode frequency of the two-ion system, to excite the motional state of trapped ions. Number of spectroscopy photons required to excite the motion depends on the Lamb-Dicke parameter, η [45, 47]. In the case of a system consists with a Ca^+ and an AlH^+ ions in an ion trap with axial secular frequency of $2\pi \times 1 \text{ MHz}$, η is around 0.15,

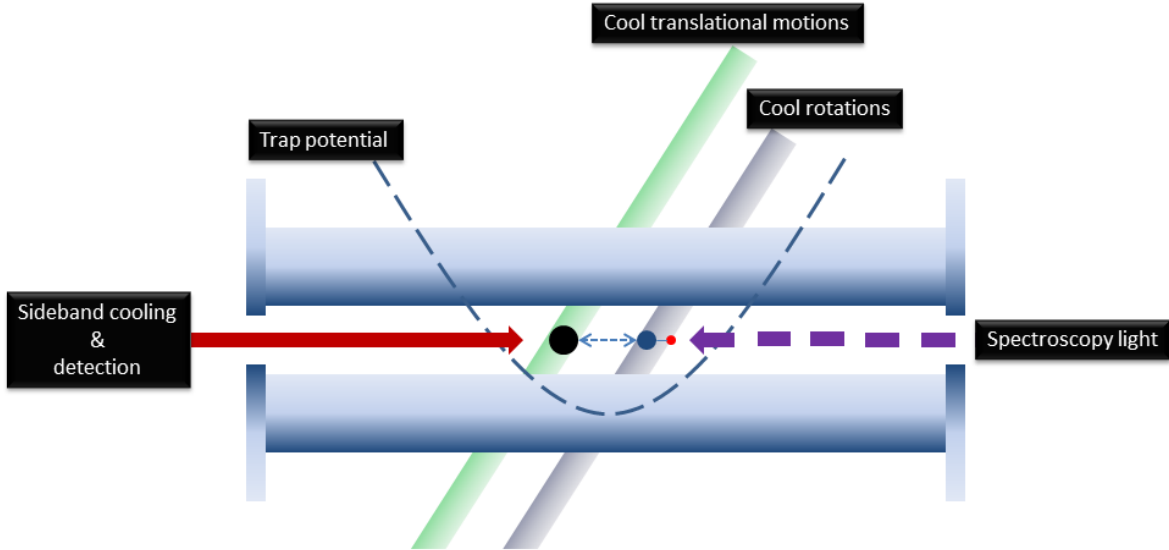


Figure 5.1. Schematics for molecular quantum logic spectroscopy (mQLS). The black dot is the atomic-logic ion, and the molecule consists of a blue and a red dot is the molecular-spectroscopy ion. The dashed curve represents the harmonic trap potential in the axial direction of the ion trap. Green and gray columns are the cooling lasers interact with logic and spectroscopy ions to cool translational and rotational motions, respectively. The red arrow from the left represents a laser utilized to perform sideband cooling and detection. The purple-dashed arrow from the right represents the spectroscopy laser to excite the COM motion of the 2-ion system.

which indicates to excite the motional states requires absorption of around 7 photons. The Franck-Condon-Factors between the electronic X and A states of AlH^+ create a semi-closed cycling allows roughly 30 cycles between the vibrational ground states before the population falling out of cycling, that are ample for a system with $\eta = 0.15$. After applying pulsed spectroscopy laser to excite the COM motional mode of the system, a laser on resonance to the red-sideband of the cooling transition of the logic ion would be

applied to verify if the system is in the excited COM motional mode, and furthermore extract the wavelength of the molecular transition of interest.

References

- [1] Herschbach, D. *Faraday Discussions* **142**, 9 (2009).
- [2] Hansen, A. K., Versolato, O. O., Kosowski, L., Kristensen, S. B., Gingell, A., Schwarz, M., Windberger, A., Ullrich, J., López-Urrutia, J. R. C., and Drewsen, M. *Nature* **508**(7494), 76–79 April (2014).
- [3] Lien, C.-Y., Williams, S. R., and Odom, B. *Physical chemistry chemical physics : PCCP* **13**(42), 18825–9 November (2011).
- [4] Lien, C.-Y., Seck, C. M., Lin, Y.-W., Nguyen, J. H. V., Tabor, D. A., and Odom, B. C. *arXiv:1402.3918* (2014).
- [5] Carr, L. D., DeMille, D., Krens, R. V., and Ye, J. *New Journal of Physics* **11**(5), 055049 May (2009).
- [6] Schmidt, P. O., Rosenband, T., Koelemeij, J. C. J., Hume, D. B., Itano, W. M., Bergquist, J. C., and Wineland, D. J. In *Non-Neutral Plasma Physics VI, Workshop on Non-neutral Plasmas (AIP Conf. Proc. 862)*, Drewsen, M., Uggerhøj, U., and Knudsen, H., editors, 305–312, (2006).
- [7] Shuman, E. S., Barry, J. F., and Demille, D. *Nature* **467**(7317), 820–823 September (2010).

- [8] Nguyen, J. H. V. and Odom, B. *Physical Review A* **83**(5), 1–7 May (2011).
- [9] Hutson, J. M. *Science* **327**(5967), 788–789 February (2010).
- [10] Ospelkaus, S., Ni, K.-K., Quéméner, G., Neyenhuis, B., Wang, D., de Miranda, M. H. G., Bohn, J. L., Ye, J., and Jin, D. S. *Physical Review Letters* **104**(3), 2–5 January (2010).
- [11] de Miranda, M. H. G., Chotia, a., Neyenhuis, B., Wang, D., Quéméner, G., Ospelkaus, S., Bohn, J. L., Ye, J., and Jin, D. S. *Nature Physics* **7**(6), 502–507 March (2011).
- [12] Hänsch, T. W. and Schawlow, A. L. *Optics Communications* **13**(1), 68–69 (1975).
- [13] Wineland, D. J. and Itano, W. M. *Physical Review* **20**, 1521–1540 (1979).
- [14] Lett, P. D., Phillips, W. D., Rolston, S. L., Tanner, C. E., Watts, R. N., and Westbrook, C. I. *Journal of the Optical Society of America B* **6**(11), 2084 November (1989).
- [15] Diedrich, F., Bergquist, J., Itano, W., and Wineland, D. *Physical review letters* **62**(4), 403–406 January (1989).
- [16] Diddams, S. a., Udem, T., Bergquist, J. C., Curtis, E. a., Drullinger, R. E., Hollberg, L., Itano, W. M., Lee, W. D., Oates, C. W., Vogel, K. R., and Wineland, D. J. *Science* **293**(5531), 825–828 August (2001).

- [17] Ni, K.-K., Ospelkaus, S., de Miranda, M. H. G., Pe'er, A., Neyenhuis, B., Zirbel, J. J., Kotochigova, S., Julienne, P. S., Jin, D. S., and Ye, J. *Science* **322**(5899), 231–5 October (2008).
- [18] Shi, W. and Malinovskaya, S. *Physical Review A* **82**(1), 013407 July (2010).
- [19] Sta anum, P. F., Høj bjerre, K., Skyt, P. S., Hansen, A. K., and Drewsen, M. *Nature Physics* **6**(4), 271–274 March (2010).
- [20] Schneider, T., Roth, B., Duncker, H., Ernsting, I., and Schiller, S. *Nature Physics* **6**(4), 275–278 March (2010).
- [21] Weiner, A. M. *Review of Scientific Instruments* **71**(5), 1929–1960 (2000).
- [22] Viteau, M., Chotia, A., Allegrini, M., Bouloufa, N., Dulieu, O., Comparat, D., and Pillet, P. *Science* **321**(5886), 232–234 July (2008).
- [23] Sofikitis, D., Weber, S., Fioretti, a., Horchani, R., Allegrini, M., Chatel, B., Comparat, D., and Pillet, P. *New Journal of Physics* **11**(5), 055037 May (2009).
- [24] Jarmain, W. R. *Journal of Quantitative Spectroscopy and Radiative Transfer* **11**(5), 421–426 (1971).
- [25] Rajagopal, V. *Trapped Ion Thermometry and Mass Determination through Imaging*. PhD thesis, Northwestern University, (2014).
- [26] Tabor, D. *Rovibrational Cooling of SiO+*. PhD thesis, Northwestern University, (2014).

- [27] Roth, B., Ostendorf, A., Wenz, H., and Schiller, S. *Journal of Physics B: Atomic, Molecular and Optical Physics* **38**(20), 3673–3685 October (2005).
- [28] Sofikitis, D., Horchani, R., Li, X., Pichler, M., Allegrini, M., Fioretti, A., Comparat, D., and Pillet, P. *Physical Review A* **80**(5), 1–4 November (2009).
- [29] Mogi, T., Fukuyama, Y., Kobayashi, T., Tanihata, I., Uehara, K., and Matsuo, Y. *Applied Surface Science* **197-198**, 202–206 September (2002).
- [30] Tong, X., Winney, A., and Willitsch, S. *Physical Review Letters* **105**, 143001 September (2010).
- [31] Seck, C. M., Hohenstein, E. G., Lien, C.-Y., Stollenwerk, P. R., and Odom, B. C. *Journal of Molecular Spectroscopy* **300**, 108–111 (2014).
- [32] Guest, M. F. and Hlrs, D. M. *Chemical Physics Letters* **84**(1), 167 (1981).
- [33] Almy, G. M. and Watson, M. C. *Physical Review* **45**, 871 (1934).
- [34] Bruna, P. J. and Grein, F. *Physical Chemistry Chemical Physics* **5**(15), 3140 (2003).
- [35] Roth, B., Blythe, P., and Schiller, S. *Physical Review A* **75**(2), 023402 February (2007).
- [36] Removille, S., Dubessy, R., Dubost, B., Glorieux, Q., Coudreau, T., Guibal, S., Likforman, J.-P., and Guidoni, L. *Journal of Physics B: Atomic, Molecular and Optical Physics* **42**(15), 154014 August (2009).

- [37] Schwartz, J. C., Senko, M. W., and Syka, J. E. P. *Journal of the American Society for Mass Spectrometry* **13**(6), 659–669 (2002).
- [38] Rellergert, W. G., Sullivan, S. T., Schowalter, S. J., Kotochigova, S., Chen, K., and Hudson, E. R. *Nature* **495**(7442), 490–4 March (2013).
- [39] Sise, O., Ulu, M., and Dogan, M. *Nuclear Instruments and Methods in Physics Research Section A: Accelerators, Spectrometers, Detectors and Associated Equipment* **554**(1-3), 114–131 December (2005).
- [40] Nguyen, J. H. V., Viteri, C. R., Hohenstein, E. G., Sherrill, C. D., Brown, K. R., and Odom, B. *New Journal of Physics* **13**(6), 063023 June (2011).
- [41] Szajna, W. and Zachwieja, M. *Journal of Molecular Spectroscopy* May (2011).
- [42] Berkeland, D. J., Miller, J. D., Bergquist, J. C., Itano, W. M., and Wineland, D. J. *Journal of Applied Physics* **83**(10), 5025 (1998).
- [43] Versolato, O. O., Schwarz, M., Hansen, A. K., Gingell, A. D., Windberger, A., Kosowski, ., Ullrich, J., Jensen, F., Crespo López-Urrutia, J. R., and Drewsen, M. *Physical Review Letters* **111**(5), 053002 July (2013).
- [44] Schiller, S. and Korobov, V. *Physical Review A* **71**(3), 032505 March (2005).
- [45] Wan, Y., Gebert, F., Wübbena, J. B., Scharnhorst, N., Amairi, S., Leroux, I. D., Hemmerling, B., Lörch, N., Hammerer, K., and Schmidt, P. O. *Nature communications* **5**, 3096 January (2014).

- [46] Wübbena, J. B., Amairi, S., Mandel, O., and Schmidt, P. O. *Physical Review A* **85**(4), 043412 April (2012).
- [47] Morigi, G., Eschner, J., Cirac, J., and Zoller, P. *Physical Review A* **59**(5), 3797–3808 May (1999).
- [48] Schulz, S. A., Poschinger, U., Ziesel, F., and Schmidt-Kaler, F. *New Journal of Physics* **10**(4), 045007 April (2008).

APPENDIX A

Machine Drawing of Apparatus

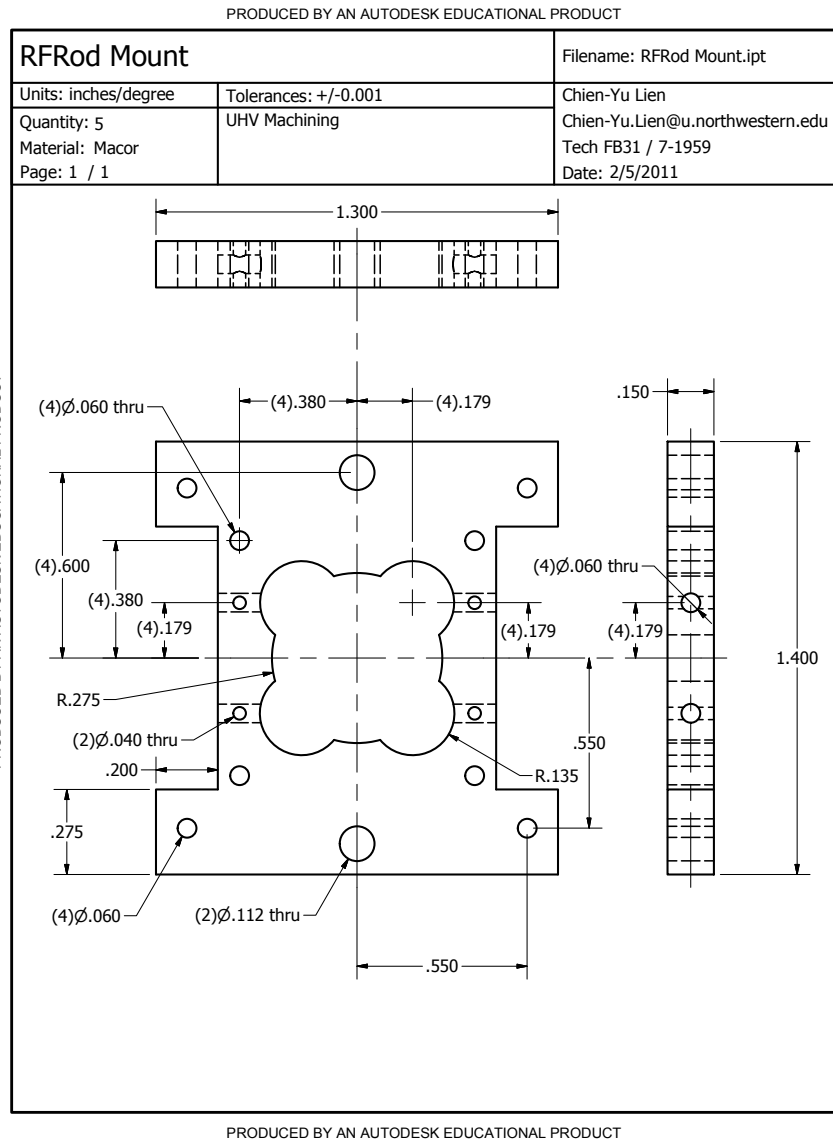


Figure A.1. RF linear ion trap mousing plate.

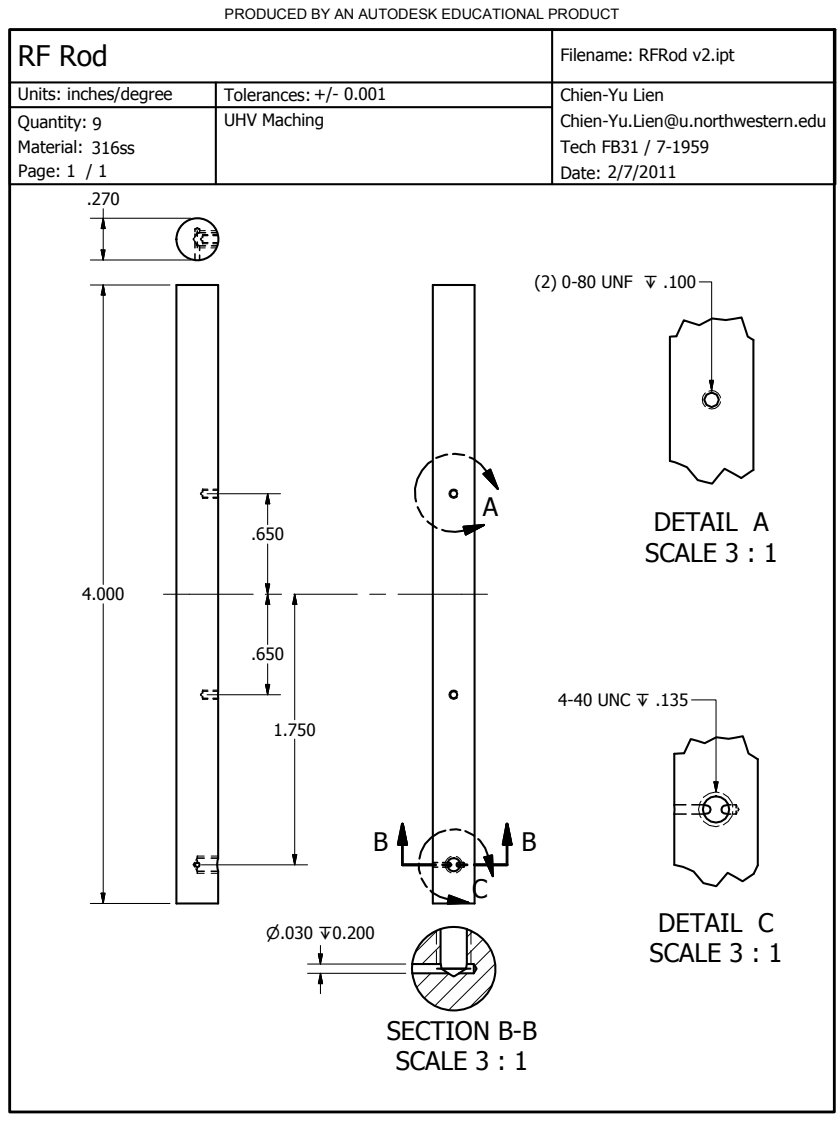


Figure A.2. RF rods.

PRODUCED BY AN AUTODESK EDUCATIONAL PRODUCT

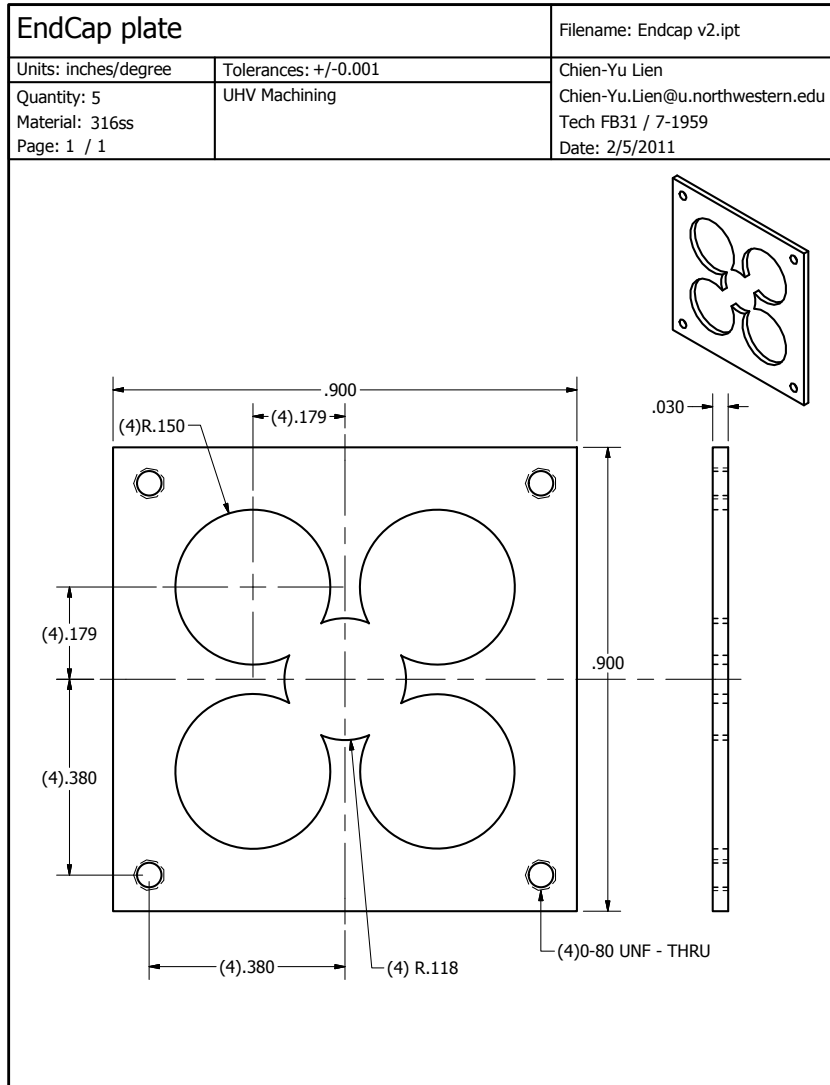


Figure A.3. Endcap plates.

PRODUCED BY AN AUTODESK EDUCATIONAL PRODUCT

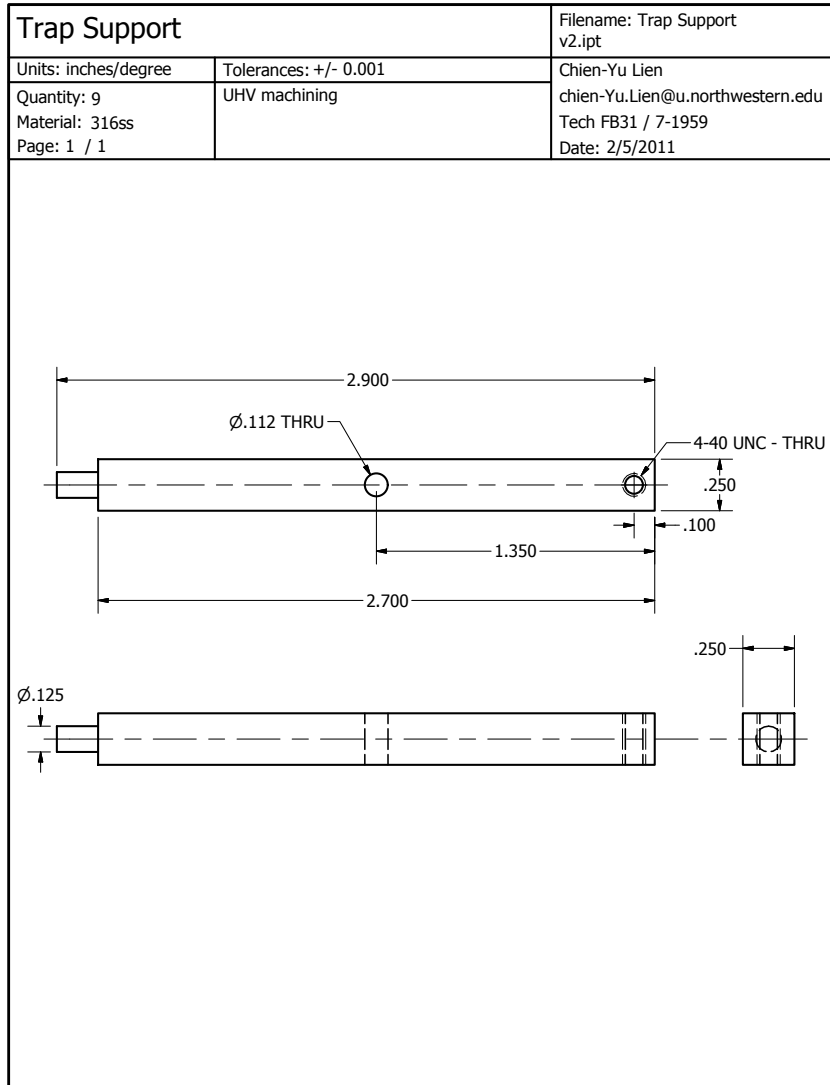


Figure A.4. Trap support.

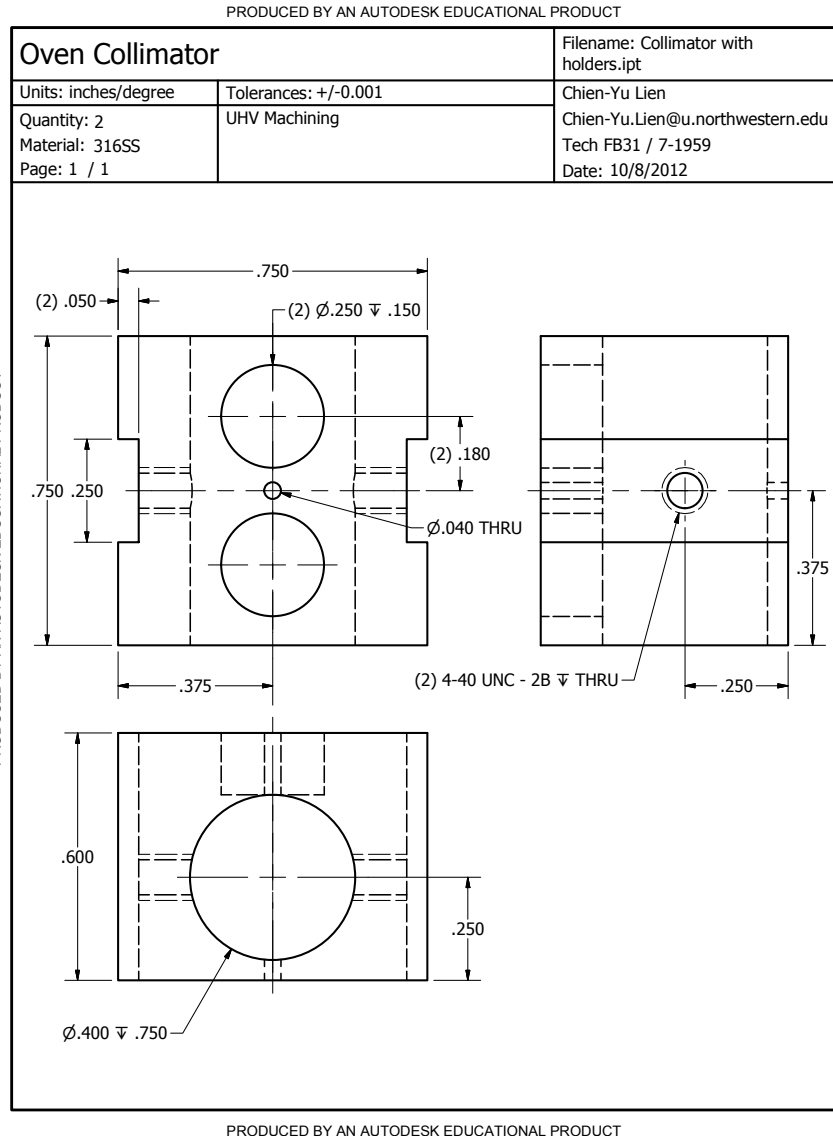


Figure A.5. Barium oven collimator integrated with ablation target holders.

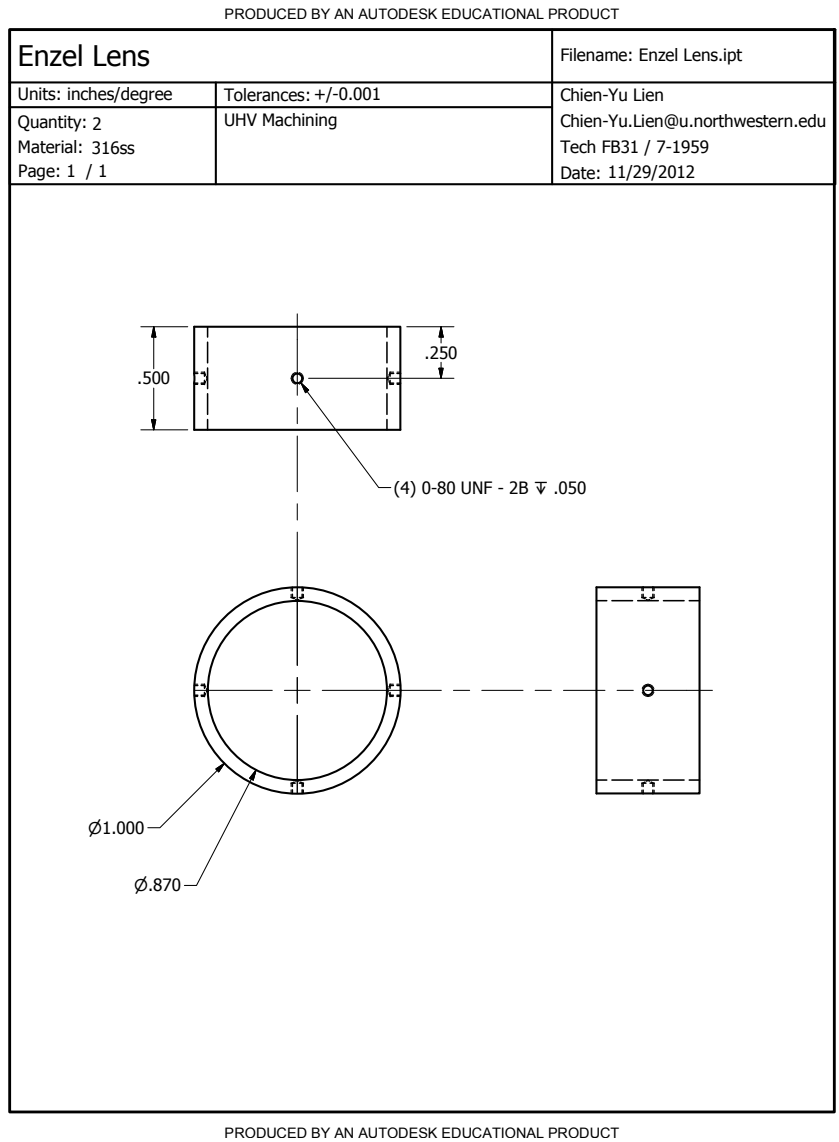


Figure A.6. One of the einzel lens rings.

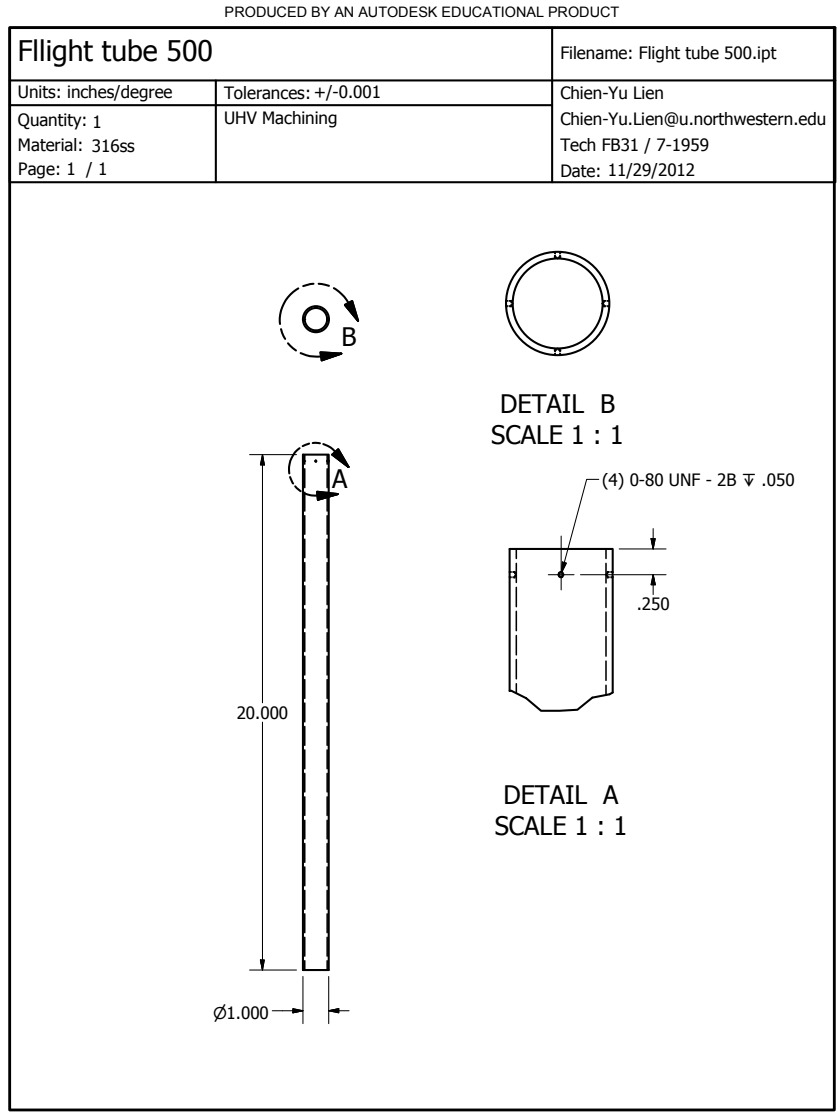


Figure A.7. 20" (~50 cm) long flight tube.

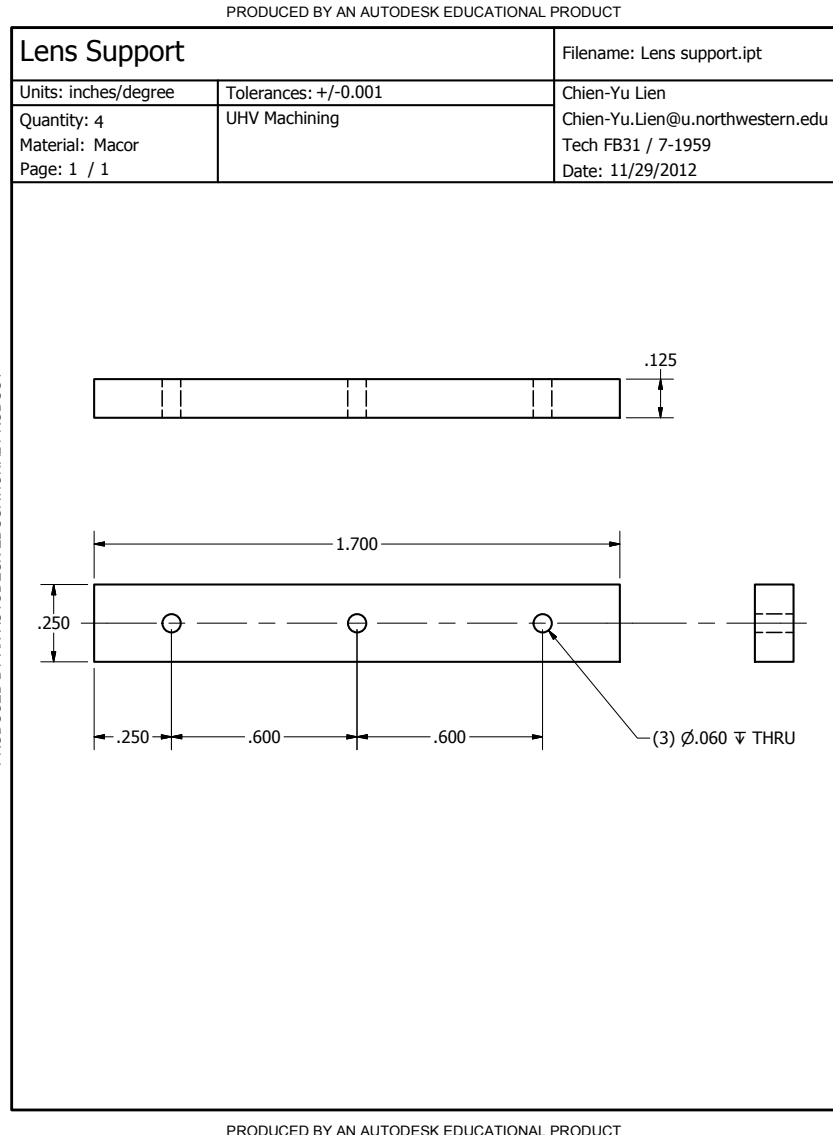


Figure A.8. Supporting bar connects einzel lens to the flight tube.

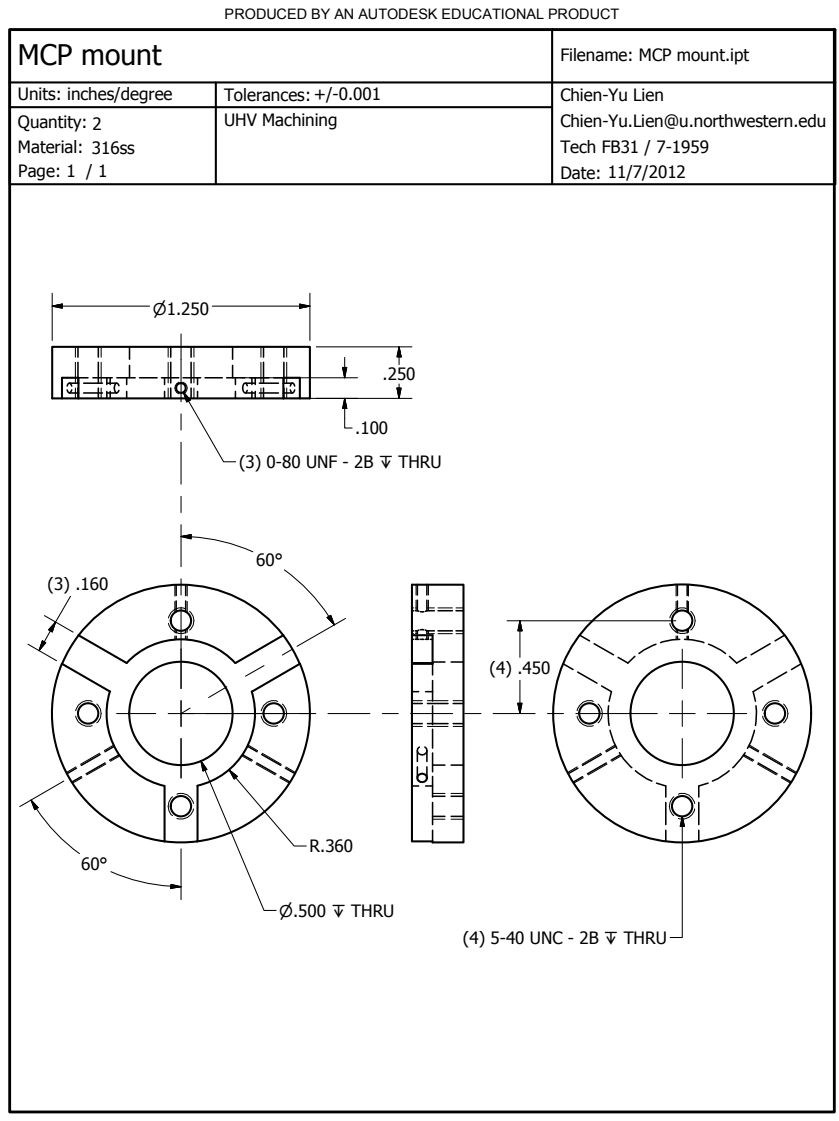


Figure A.9. MCP (Hamamatsu F4655) mount.

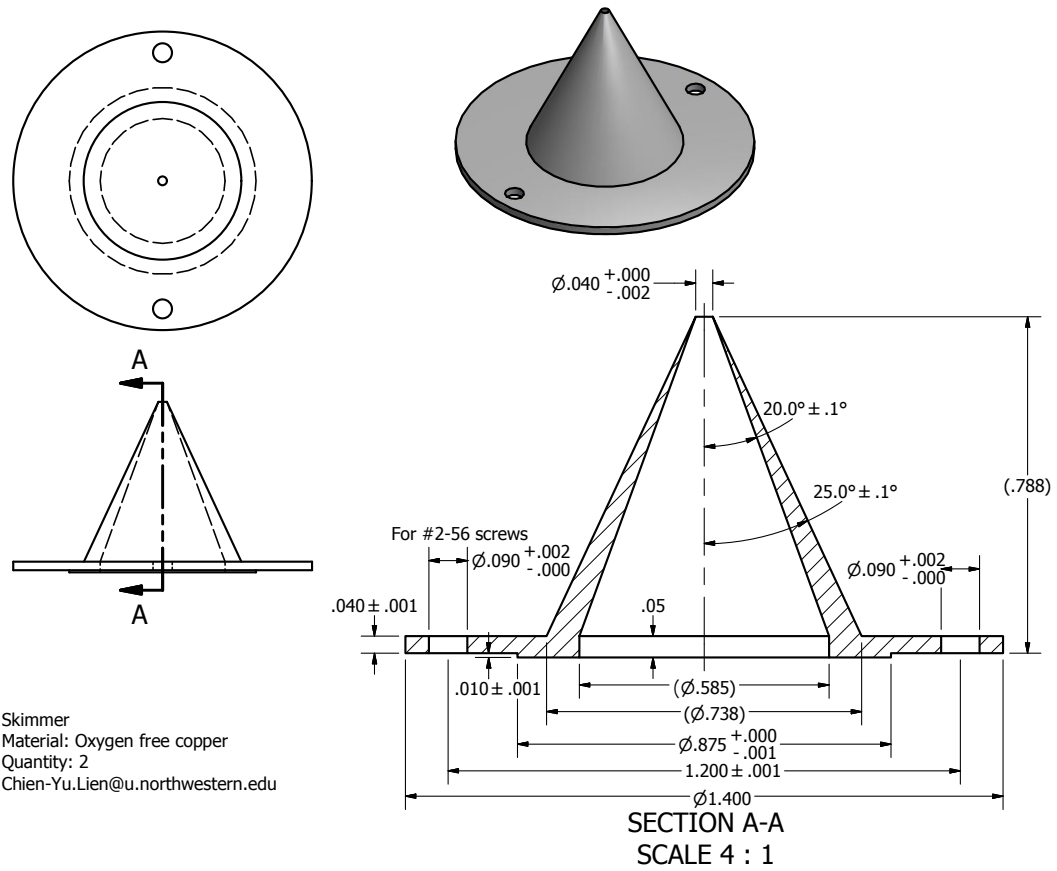


Figure A.10. Skimmer. Material of the skimmer was replaced from oxygen free copper to 316ss for durability and easier machining.

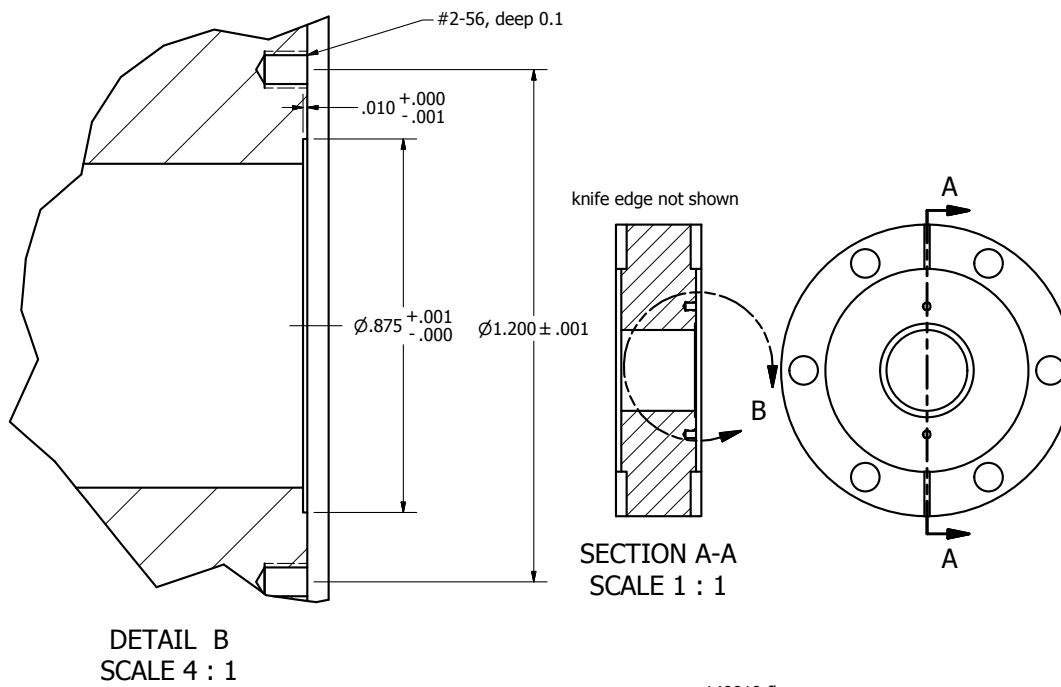


Figure A.11. Modified MDC 140010 flange for holding and aligning skimmer.